EXPERIMENTAL INVESTIGATION OF NOISE INDUCED TRANSITIONS IN THERMOACOUSTIC SYSTEM

A THESIS

submitted by

VIVEKANANDAN JEGADEESAN

for the award of the degree

of

MASTER OF SCIENCE

(by Research)

DEPARTMENT OF AEROSPACE ENGINEERING
INDIAN INSTITUTE OF TECHNOLOGY MADRAS

JULY 2012

THESIS CERTIFICATE

This is to certify that the thesis titled **EXPERIMENTAL INVESTIGATION OF NOISE INDUCED TRANSITIONS IN THERMOACOUSTIC SYSTEM**, submitted by **Vivekanandan Jegadeesan**, to the Indian Institute of Technology, Madras, for the award of the degree of **Master of Science**, is a bona fide record of the research work done by him under my supervision. The contents of this thesis, in full or in parts, have not been submitted to any other Institute or University for the award of any degree or diploma.

Prof. R. I. Sujith
Research Guide
Professor
Dept. of Aerospace Egineering
IIT-Madras, 600 036

Place: Chennai

Date: 6^{th} July 2012

ACKNOWLEDGEMENTS

I would like to thank and acknowledge all the people who helped me during my three years of research. The last three years have been my most enlightening in my life. During the years, I was able to meet lot of high calibre people and admired about their quality and achievements.

First I would like to thank my supervisor, Prof. R. I. Sujith for trusting in me and providing me an opportunity to work in this great lab. I always admired at the level of care he showed towards his students and the way he guided us, which motivated us to work hard. Without him I would have ended as a mediocre engineer in a production plant. He shaped my career and taught lot of things, both academic and non-academic which helped me to understand the essence of research.

I would like to express my gratitude to General Test Committee members, Prof. S. R. Chakravarthy for guiding me in fabricating my experimental setup and Prof. Babu Viswanathan for valuable suggestions and comments during the meetings. I would like to thank our HODs, Prof. P. Sriram and Prof. V. Bhaskar for valuable guidance and support they provided me during my stay. I would also like to express my gratitude to my teachers, Dr. P. A. Ramakrishna, Dr. S. Sarkar, Prof. R. Velmurugan, Prof. K. Bhaskar, Dr. A. Sameen and Dr. H. S. N. Murthy for their immense patience to teach me the basics of Aerospace Engineering and helped me to understand better.

I am indebted to Dr. Muruganandam for answering patiently to my doubts regarding heat release rate measurement. His guidance helped me to understand about measurement of heat release rate and aided me in setting up the instrumentation. I wish to thank Prof. Wolfgang Polifke (Technische Universität München), for his critical comments during his visits, which helped me think better and understand better. I would like to thank Dr Ramanarayanan (University College London) for providing me with valuable information on setting up a laminar flame.

During my stay, I have greatly benefited by attending the AIM meetings held at IIT Madras and JNCASR, organized by Dr. Matthew Juniper (University of Cambridge) and my advisor. The valuable discussions during the meetings helped me in understanding about stability of a system and its prediction. In these meetings, the discussion I had with Ian waugh (University of Cambridge) were very fruitful and helped me in understanding about stochastic dynamical system. I also like to thank Dr. A. Kushari (IIT Kanpur) and Mr. Sandeep (IIT Kanpur) for conducting the crash course on Laser Doppler Velocimetry which greatly helped me in my investigation.

During my stay, I have been supported constantly by administrative staff, Mr. Sundar, Mrs. Mekala, Mr. Dhanapal, Mr. Stephen, Mr. Siva, Ms. Rajalakshmi, Ms. Pavitra during my paper work. I would like specially thank Mr. Shankar Kumarasamy and Mr. Kennedy for aiding me workshop, procuring materials and accessories for my project. I am greatly indebted to Mr. Ranganathan and Mr. Chandru for their excellent fabrication of most of the components in my experimental setup.

It would be injustice, if I do not mention the contribution from my lab mates. My friends in the lab have been a great support to me at the time of distress. They guided me through some of the dark periods during my stay and turned it into a pleasant experience. First I would like to thank Dr. S. Priya and Dr. M. Sathesh for spending their valuable time and effort, to teach me non-linear dynamics (I would like to emphasize that it is not that easy to teach me). Dr. S. Priya (Chinna Akka - this will irritate her) spent hours talking to me and guided me through some confused times during my stay. I had great opportunity to interact with Dr. M. Sathesh (my buddy), with whom I spent most of my time and talked and argued on lot of non-academic stuff and sufficiently lot of academic stuff too. I would like to thank Ramgopal, Rajinikanth and Roopa for providing me with vital support in my research and the great time I had spent with them. Without the valuable inputs from Gireesh sir (Symbol of peace and patience), Vineeth nair, Vikrant and Joseph my research would not have got completed. I would like to thank Avishek, Lipika (Akka aka Periya Akka), Irfan, Trinath, Rajesh, David, Pushkarini, Gopalakrishnan, Ayanath, Vishnu, Meenakshi and Harshini for sharing their time and the pleasant experiences.

I wanted to specially thank Gireesh sir and Balaji anna for teaching me how to be

patient in life. I also wanted to thank Mr. Rajasekar, my metallurgy teacher from my undergraduate school for letting me know about the M. S. Program in IIT Madras.

Overall, I would like to acknowledge that all what I have achieved in my life is due to my parents and my brother. My parents and my brother sacrificed their life to provide me with the best education and opportunities in my life. I thank God, for blessing me with good health and good people in my life.

ABSTRACT

KEYWORDS: Thermoacoustic instability; Noise induced transition; Triggering; Non-premixed flame; Stochastic stability.

Thermoacoustic instability has been observed in high intensity and high performance combustion systems. Under suitable circumstances, the fluctuating heat release rate can couple with the acoustic field in combustion system and leads to sustained oscillations. The resulting oscillations are so intense, that they damage the components associated with the system. The occurrence of thermoacoustic instability can be classified in to two types: soft and hard excitations. When the oscillations start spontaneously in the combustion chamber, the instability is said to be softly excited. In hard excitation a large amplitude disturbance has to be imparted to initiate oscillation. In order to hard excite a combustion system the disturbance has to be above a threshold level called triggering amplitude. This phenomenon is called as triggering.

The occurrence of instability has been observed to have a probabilistic nature. The probabilistic nature is attributed to the randomness of the process that occur in the combustion system. The chances of noise inducing instability in a system has been extensively studied in fields like physics, chemical and biological system.

In the present thesis, the effect of noise on the stability of a thermoacoustic system operating in a bistable region is experimentally investigated. The thermoacoustic system chosen for investigation is a ducted non-premixed flame. The system is excited by random fuel flow rate fluctuations which affects the system dynamics as parametric noise. Under the influence of noise, the system undergoes transition from stable to oscillatory state. In particular, transition is observed even when the amplitude of the noise is significantly less than the triggering amplitude of the corresponding deterministic system. While triggering from noise of low amplitudes, phase portraits reveal that the system evolves transiently towards an unstable periodic orbit, before eventually grow-

ing to a stable periodic orbit. A stochastic stability map is constructed to represent the probability of the system to undergo transition. It is also observed that the amplitude of the oscillatory state is affected by the noise level.

TABLE OF CONTENTS

LIST OF TABLES

LIST OF FIGURES

ABBREVIATIONS

NIT	Noise Induced Transition
PMT	Photo Multiplier Tube
DAQ	Data Acquisition
THD	Total Harmonic Distortion
ULC	Unstable Limit Cycle
SLC	Stable Limit Cycle
HS-PIV	high Speed Particle Image Velocimetry
LDV	Laser Doppler Velocimetry
PDF	Probability Density Function

NOTATION

Re	Reynolds number
$Re_{critical}$	Critical Reynolds number
α	Decay rate s^{-1}
P'	Instantaneous amplitude of pressure oscillation observed in the combustion chamber Pa
X_f	Location of flame inside the tube cm
$\bar{q}$	Mean heat release rate
q'	Fluctuating heat release rate
$\dot{Q}$	Volume flow rate of fuel from brass tube m^3/s
ϕ	phase difference between pressure fluctuation and heat release rate $degree$
V_{avg}	spatially averaged velocity m/s
$\bar{V}_{avg}$	Temporo-spatial avaraged velocity m/s
$V_a'vg$	Instantaneous spatially averaged velocity m/s
V_{max}	Center line velocity m/s
V'_{max}	Instantaneous center line velocity m/s
$\bar{V'}_{max}$	temporally averaged center line velocity m/s
$P'_{rms(pc)}$	Standard deviation of the pressure fluctuation observed inside the plenum chamber Pa
P'_{rms}	Standard deviation of the pressure fluctuation observed inside the combustion chamber Pa
Γ	variation of acoustic driving energy
ζ	strength of coupling between pressure fluctuation and heat release rate

CHAPTER 1

INTRODUCTION

1.1 Historical overview

Thermoacoustic instability was first observed by Higgins in 1777 (Higgins, 1802), and it was referred to as 'singing flames'. This was accidentally discovered by Higgins when he attempted to prove that water is produced when hydrogen is burnt in air. He placed a Hydrogen diffusion flame inside a confinement in an attempt to collect the condensate, but instead he observed a distinct tone from the confinement. Rijke (1859*b*) extensively investigated this phenomenon and showed that heat source inside a confinement (vertical tube) can excite the acoustic field in it and sound can be produced. He used a heated wire gauze as a heat source in his experiments. The sound produced was maximum when the gauze was located 0.2 times the length of the duct from the bottom. The oscillations were sustained as long as there was a mean flow in the system. Similar kind of oscillations was observed by glass blowers and it was reported by Sondhauss (Sondhauss, 1850). Unlike Rijke's experiment, the oscillations in a Sondhauss tube were established in a acoustically closed-open duct and didn't require a mean flow to sustain the oscillations.

Moreover sound can also be generated when there is a suitable heat sink present in the system. Johannes Bosscha, Rijke's assistant observed that the oscillations were sustained when a cooled wire gauze (heat sink) was placed at 0.8 times the length of the duct similar to the one used by Rijke (Rijke, 1859*a*). Similar to Rijke tube the oscillations were sustained only when there was a mean flow in the system. An equivalent of the Sondhauss oscillations were observed by Taconis *et al.* (1949) in a closed open cryogenic vessel. The oscillations were observed in a Helium gas filled closed-open vessel, when its open end was cooled to cryogenic temperature and the closed end was maintained at room temperature. Thus thermoacoustic oscillations occur, when there is a suitable temperature gradient and acoustic field in a system.

Rayleigh (Rayleigh, 1878) hypothesized a criterion for oscillations to be sustained by heat release/removal rate fluctuation and thus providing a condition for predicting the onset of instability. In his criterion Rayleigh stated that *"if heat is periodically communicated to, and abstracted from, a mass of air vibrating in a cylinder bounded by a piston, the effect produced will depend upon the phase of the vibration at which the heat transfer takes place. If heat is given to air at the moment of greatest condensation, or taken from it at the moment of greatest rarefaction, the vibration is encouraged. On the other hand, if heat is given at the moment of greatest rarefaction, or abstracted at the moment of greatest condensation, the vibration is discouraged"*. This is mathematically expressed in Eqn. 1.1 (Deckker, 1970).

$$\int_0^T \int_0^V \hat{P}'(x,t).\hat{q}'(x,t)dvdt > o \tag{1.1}$$

where the $\hat{P}'$ represents the pressure fluctuations and $\hat{q}'$ represents the heat release rate fluctuations in the system, V represents the volume of the system and T represents the time period of oscillation.

1.2 Impact of thermoacoustic oscillation

The phenomenon of thermoacoustic instability changed from academic interest to a plaguing problem after the advent of the high intensity combustion systems (Zinn and Lieuwen, 2006). As the industrial requirement grew larger, so did the the requirement for power. To meet the demands, high intensity combustion systems were developed which were often observed to experience thermoacoustic oscillations. Especially thermoacoustic oscillations became a major obstacle in the development and operation of liquid rocket engines (LRE) and in gas turbine engines. The oscillations observed in such systems were so large that they destroyed the components associated with the combustion systems. In some cases, the oscillations could lead to catastrophic failure of the entire system. For example F1 rocket engines development were plagued by thermoacoustic oscillations and in many cases the engines catastrophically failed during testing (Harrje and Reardon, 1972). It almost took 7 years and 2000 test runs to fix the

problem.

During thermoacoustic oscillations, the pressure oscillations in the chamber are so large that they exert fatigue loads to the structure of the system. Under the influence of oscillations the heat release rate in the system is enhanced which leads to excessive heat loads. Moreover the velocity oscillations in the system reduces the thickness of the boundary layer and increases the heat transfer to the walls leading to premature failure of combustion liner and the other associated components (Komarov and Hirasawa, 2003). Thermoacoustic oscillations also result in power and thrust fluctuations, in some cases the frequency of oscillations could be in resonance with other component in the system leading to amplitude build up (Norton and Karczub, 2003). Hence in general thermoacoustic oscillations are not preferred in a combustion system.

On the contrary, there are also cases in which thermoacoustic oscillations are encouraged, for example Lennox air heaters, Argus As 109-014 pulse jet engine, Reynst pulverized coal and oil fired furnaces are to name a few (Reynst, 1961). The ability of the oscillatory flow field to increase the heat transfer was utilized in the lennox air heaters and slurry dryers, making the system more compact and more efficient. Reynst (1961) designed and built pulsating combustors to burn pulverized coal, the pulsating combustor utilized the intense oscillations to enhance the burn rate of the coal and reduced the pollutant emission. Germans developed Argus 109-014 pulse jet engines to propel small aircrafts and unmanned flying bombs (V1) which utilized the thermoacoustic oscillations self-sustainability to eliminate the need for the compressor and turbines for the operation of jet engines. Thus, Thermoacosutic oscillations are not always considered as a nuisance; they are also desirable at times (Putnam *et al.*, 1986).

1.3 Mechanism of oscillation

Thermoacoustic oscillations occur in a system whenever a positive feedback loop is established between the fluctuating heat release rate and the acoustic field in the system (Putnam, 1971). The fluctuating heat release rate in the system act as a source of energy and the acoustic field in the system acts as a feedback circuit to sustain the oscillations

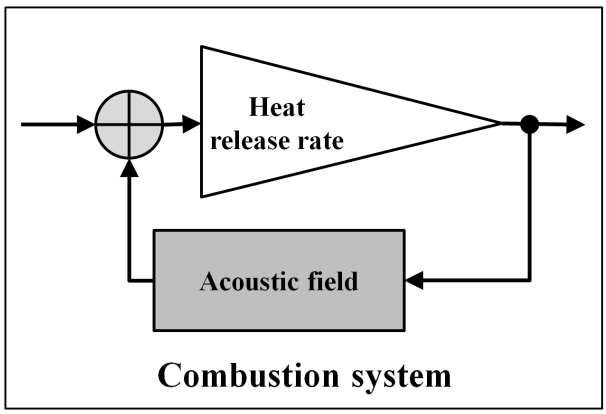

Figure 1.1: Schematic representation of feedback mechanism in combustion system

(see Fig. 1.1). There are large number of sources for heat release rate fluctuation, to name a few; fluctuations in the fuel mass flow rate, fluctuation of flame area and flame wrinkling, the dependency of heat release rate on pressure, unsteady fuel atomization, equivalence ratio fluctuation etc (Putnam, 1971).

Fluctuation in the mass flow rate of fuel lead to fluctuation in equivalence ratio. The fluctuating equivalence ratio can further lead to fluctuation of heat release in the system, which in turn generates pressure disturbances. The pressure disturbances are reflected back from the walls of the combustor to the fuel injectors. The reflected pressure disturbance influences the fuel flow and further enhances the mass flow fluctuation, this again affects the heat release and generates pressure disturbance. Under suitable condition, the mass flow fluctuation can couple with the acoustic field and can lead to sustained oscillations (Jones, 1945). The frequency of oscillations need not necessarily be the natural mode of the system. This type of coupling is often observed in furnaces and room heaters (Putnam *et al.*, 1967). The coupling of fuel flow fluctuation to acoustics can be avoided by choking the fuel injectors.

Even after chocking the fuel flow lines the velocity fluctuation in the air flow lead to equivalence ratio fluctuation. The velocity fluctuations present in the plane of injection causes a fluctuation in the mass flow rate (across the injection plane), this leads to equivalence ratio fluctuation and heat release rate fluctuation. As explained earlier, the equivalence ratio fluctuation can couple with the acoustics in the system. This type of coupling is often observed in gas turbine combustors. The coupling can be prevented

by placing the fuel injector at a suitable position.

The fluctuation of flame area can be caused by equivalence ratio fluctuation, hydrodynamic fluctuation and inlet mixture temperature fluctuation. Fluctuation in flame area leads to fluctuation in heat release rate, thus generating pressure disturbances. When the generated pressure disturbances impinges back on the flame, it leads to Taylor-Markstein instability and further enhances the heat release rate of the flame (Markstein and Squire, 1955). This kind of coupling is often observed in low NoX combustors.

The heat release rate of a mixture of fuel and oxidizer depends upon the pressure of the environment (Putnam and Dennis, 1955). If the response of the combustible mixture is such that the it enhances the heat release rate of the system as the pressure increases, it would lead to coupling of acoustic field in the combustion system and heat release rate. This kind of coupling is often observed in solid rocket booster motors.

The atomization of fuel droplets are affected by the pressure and velocity fluctuation present at the injection plane (Sujith, 2005). The pressure fluctuation at the injectors fluctuates the pressure drop across the injectors, this leads to uneven fuel droplet distribution. Similarly the velocity fluctuation at the injectors affects the shearing of the droplets leading to droplet size fluctuation, mixing and mass transfer. The heat release at the combustion chamber depends on the droplet size and mixture fraction. Thus the unsteady atomization can lead to unsteady heat release rate, which on coupling with the acoustic field could lead to a sustained thermoacoustic oscillation. This type of coupling is observed in gas turbine engines, ramjet engines and liquid rocket engine.

1.4 Onset of instability

A large amount of effort has been invested to predict the onset of thermoacoustic instability. Thermoacoustic oscillations can be investigated through dynamical system approach. The onset of instability, nature of transition to instability and nature of oscillations can be investigated and the stability of the combustor can be represented through phase space and bifurcation diagram. Phase space is defined as space in which all possible states of the system is represented. The evolution of the system is represented by

the trajectories in the phase space (Strogatz, 2000).

The onset of thermoacoustic oscillations in a combustion system can be of two types: soft and hard excitation (Burnley and Culick, 2000). A spontaneous transition from infinitesimally small disturbance to self-sustained oscillations is referred to as soft excitation or linear instability. This is observed when the operating conditions of the system are varied beyond its linear stability margin. The condition at which the system becomes linearly unstable can be predicted using linear stability analysis (Perko, 2009).

A stable combustor (one that does not oscillate spontaneously) can be "triggered" into self-sustained oscillation by exciting the system with a finite amplitude disturbance. This phenomenon is referred to as hard excitation or triggering instability, or subcritical transition to instability in the dynamical systems parlance. During triggering, the thermoacoustic system evolves from a finite amplitude disturbance (a hard excitation) above a threshold amplitude called "triggering amplitude" (Crocco and Cheng, 1956). When the amplitude of the initial condition is less than the triggering amplitude, the system evolves asymptotically to a stable state. The phenomenon of triggering is observed when the system is operating in a hysteretic region of the stability map.

Similarly when the system is operating in a hysteretic region, transition from stable to oscillatory state can occur in a combustion system due to random fluctuations (noise) of the processes occurring in the combustor. Zinn and Lieuwen (2005) remark that thermoacoustic systems can undergo transition to instability by low-amplitude disturbances that are of the order of the background noise level. Transition of the system from random fluctuations to discrete monotone oscillations was often observed during the testing of liquid rocket engines (Dranovsky, 2007). The occurrence of this transition has a probabilistic nature. The system operating in steady stable state experiences an increase in the amplitude leading to self-sustained oscillations. A unique feature of this probabilistic transition is lack of reproducibility, even for same operating conditions. The source for noise in a combustion system could be from turbulence in the flow field, unsteadiness of the flow reversal, unsteadiness of mixing, to name a few (Burnley and Culick, 2000). The phenomenon of system undergoing transition from stable to unstable state under the influence of the noise is called noise induced transition (NIT). NIT has been extensively investigated by Horsethemke and Lefever (1984) for chem-

ical and electrical systems. They found that NIT plays a critical role in the stability of the system; yet only a limited amount of work has been performed in the field of thermoacoustics.

CHAPTER 2

LITERATURE REVIEW

Initially it was belived that nature is deterministic and predictable, hence randomness or noise were considered to be an obstacle which hindered the accurate prediction of the events. Noise was first thought of as a fluctuations from a system which has infinitely large number of degrees of freedom but their origin was unknown. Thus to understand how noise can affect the evolution, first we must understand how noise interacts with the system. A detailed description of characteristics of noise, its interaction with the system and the consequences are explained in this chapter.

2.1 Measurement and parametric noise

Noise is generally classified into measurement and parametric noise. Measurement noise are the systematic errors involved in the observation of the system; they have no impact on the system other than just blurring the trajectories of the system in phase space. Parametric noise is the randomness associated with control parameters that govern the dynamics of the system itself. The randomness could be from internal sources such as thermal noise or from external sources like fluctuations from environment.

Parametric noise is further classified into two types depending upon the manner in which it interacts with the system: additive and multiplicative noise. The evolution of the dynamical system with additive noise is expressed mathematically as in the Eqn. 2.1.

$$\frac{d\chi}{dt} = A\chi + \eta(t) \tag{2.1}$$

where χ represents the state vector of the system and Arepresents the evolution operator of χ, and η represents a parameter (vector) who's value varies randomly in time. The random fluctuations in the system is independent of the state variable of the system. On

the other hand multiplicative noise is expressed as in the Eqn. 2.2.

$$\frac{d\chi}{dt} = A\chi + B(\chi)\eta(t) \tag{2.2}$$

where B represents the evolution operator of the noise η and it is a function of χ. Here the random fluctuations depend on the state of the system. From the above explanation it is observed that the parametric noise has a profound impact on the evolution of the system, especially when the interaction is multiplicative in nature over additive (Balakrishnan, 2008).

2.2 Effect of noise on dynamics of the system

2.2.1 Numerical investigation

It was observed that addition of parametric noise has a profound effect on the dynamics of the system. Horsethemke and Lefever (1984) observed that addition of parametric noise to a deterministic non-linear system modifies the bifurcation behavior and in some cases they are observed to change the nature of bifurcation. Parametric noise perturbs the state variable such that it induces fluctuations in the energy states of the fixed points. Depending upon the noise level, the property of the fixed point is modified.

Meunier and Verga (1988) theoretically investigated the effect of noise on the nature of bifurcation. They considered a simple system which exhibited a supercritical pitchfork bifurcation to which they added Gaussian white noise. They observed that the transition in the system does not occur sharply at a critical value, instead the transition became smooth. This leads to a fuzzy bifurcation. They also observe that the transition itself occurs with a probabilistic nature. They even proposed that a system in the presence of noise cannot have critical value, instead it has a critical region where it becomes unstable. The area of the region depends on the noise level of the system.

Arnold (1998) theoretically showed that a system, whose deterministic state is defined as stable can destabilized by addition of noise. He showed that a system with random fluctuations exhibited order formation, leading to large scale dissipative struc-

tures. Further he showed that the critical value for threshold of stability itself depends on the noise level present in the system. This was also observed by Hutt (2008) in his numerical investigation. When an additive noise is added to a non-linear system he observed that the critical value of bifurcation advances as the noise level in the system increases for a system undergoing subcritical Hopf bifurcation.

Hwang *et al.* (2000) numerically studied an optically injected semiconductor laser model, and they considered the intrinsic spontaneous-emission noise for investigation. The system was observed to exhibit periodic oscillations in the absence of noise, as the noise level was increased the periodic oscillations of the system transitioned to chaotic oscillation. Thus the system was observed to exhibit noise induced chaos. The addition of noise were observed to significantly affect the system even beyond the onset of instability for a multi-dimensional system.

Similarly, Zaikin and Kurths (2000) in their numerical investigation also showed that additive noise can induce noise induced transition in the system. They investigated a Swift-Hohenberg coupling and showed that the additive noise can cause orderliness and pattern formation in the system.

Lindner *et al.* (2004) presented an elaborate numerical investigation of the effect of noise on an excitable system. He chose a FitzHugh-Nagumo and leaky integrate & fire model and studied the phenomenon of noise induced oscillation, stochastic resonance, noise induced phase transition and noise induced pulse propagation. They observed that oscillations were sustained in the system as the noise level is increased, though the fixed points were stable in nature for the deterministic case. They also investigated a model of a laser and observed the phenomenon of spiking. As the noise level was increased the number of spikes observed in the system also increased.

Ibrahim (2006) presented an assessment of the noise induced transition phenomenon in dynamical systems. He investigates the phenomenon of stabilization of a linearly unstable system through random parametric excitation. He observed that through random parametric excitation the critical value of bifurcation can be shifted to a higher value for a model that describes ship roll. In the presence of noise he also observed that the dynamics of system slow down as the operating conditions approached the Hopf point.

2.2.2 Experimental investigation

Kabashima *et al.* (1979) experimentally investigated the phenomenon of NIT in a degenerate parametric electrical oscillator. The parametric oscillator considered for investigation exhibited transition to instability via supercritical Hopf bifurcation. He showed that the critical value for the threshold of linear stability recede as the noise level in the system increases, thus increasing the stability margin of the system. He experimentally showed that an unstable fixed point was modified to a stable fixed point under the influence of noise. He also showed that a system under the influence of noise exhibited higher damping when compared to the noise free case. Similar investigation was performed by Resch *et al.* (1991) in a Methyl blue-oxygen-Sulfide oscillator. The oscillator in the present case exhibited subcritical Hopf bifurcation. The system was observed to get triggered into an oscillatory state under the influence of noise.

Juel *et al.* (1997) investigated the effect of noise on pitchfork and Hopf bifurcation experimentally and numerically. They considered a parametric oscillator similar to the one used by Kabashima *et al.* (1979). They showed that for the system under the influence of noise, the response probability density function broadened as the operating conditions approached the critical value (Hopf point). This broadening was due to the excitation of the natural modes by noise and thus increasing the sensitivity of the system to fluctuations. They also showed that the noise amplifies the inherent imperfections present in the system.

Broussell *et al.* (1997) experimentally investigated the effect of Markovian dichotomous noise in a ZnSe interference filter excited by an argon ion laser. The noise was added to the experiment through an acousto-optic modulator. For a noise free case, the system exhibited bistability in the variation of transmittance with incident power. For low noise level, they observed a single peak in the response PDF. As the noise level is increased, the single peak in the response PDF was observed to split into two peaks and the system was observed to transition between the two states in a random manner. Further increasing the noise level, the PDF further splits and finally exhibits three peaks in the response PDF. Under the influence of noise, the system was observed to sustain a third oscillatory state which was not observed in deterministic state. Thus the system

is exhibiting noise induced transition first and then it exhibits noise induced states for higher noise levels.

Residori *et al.* (2002) and Berthet *et al.* (2003) performed investigations on the effect of multiplicative noise on the stability of the system in two experimental setups. One was a RLC circuit and the other was a surface wave generated by vertically vibrating layer of fluid or Faraday instabilities. In both the experiments, they observed that the system was triggered to oscillations even before the threshold of linear stability. Further, they also reported that the noise detunes the system from forcing and reduces the amplitude of oscillation. They also observed that the system underwent transition through subcritical Hopf bifurcation in the presence of noise. In the absence of noise supercritical Hopf bifurcation was observed.

Oh and Ahlers (2003) performed experiments in a Rayleigh-Bénard cell filled with Sulfur hexafluoride (SF_6) near the critical temperature of transition. They showed experimentally that the system undergoes subcritical transition under the influence of random fluctuations, instead of undergoing a supercritical transition as with the case of the noise free system. This was theoretically predicted by Swift and Hohenberg (Swift and Hohenberg, 1977; Hohenberg and Swift, 1992).

Billings *et al.* (2004) experimentally and numerically investigated the effect of noise on acousto-optic modulated CO_2 laser. The system was observed to transition from periodic limit-cycle oscillations to noise induced chaos as the noise level in the system was increased.

2.3 Effect of noise on combustion chamber

In an effort to predict the onset of instability, large number of theories have been proposed. However the proposed theories are less accurate in predicting the stability margin of a combustion system. The theories consider all the process that occur in the combustion chamber and are assumed to behave deterministic in nature, which is not true. Inside a combustion chamber, turbulence in the flow, mixing of fuel and oxidizer, combustion of reactants etc., are random in nature and can act as a source of noise. The

randomness of the process can impart probabilistic nature to the system and affect the dynamics (Dranovsky, 2007).

Burnley and Culick (2000) theoretically investigated the effect of random fluctuations on the stability of the combustor. In their investigation they considered the noise generated due to vorticity and entropy fluctuations in the system. They identified the possibility of triggering due to random fluctuations in the system. Their investigation showed that the presence of nonlinear gasdynamics alone is not sufficient for Noise induced triggering to occur, it requires nonlinear combustion also to be present for triggering to occur.

Lieuwen and Zinn (2002) experimentally observed that lean premixed combustor operating in a stable region, but close to the critical point experienced sudden increase in the amplitude of oscillations and reach a steady oscillatory state. Lieuwen and Banaszuk (2005) further numerically investigated the effect of noise on the stability of the system. They showed that the linear stability margin of a thermoacoustic system shrinks as the noise level in the system increases. They also showed that a noisy combustion interaction between flow and heat release rate has a significant effect on the system for fluctuations as low as $u'_{rms}/\bar{u} \sim 5\%$.

Balasubramanian and Sujith (2008*a*,*b*) showed that thermoacoustic systems are non-normal in general. They were the first to identify the non-normality of the thermoacoustic system and investigated its consequences. They observed that conventional stability analysis is not sufficient to describe the stability margin of the thermoacoustic system with non-normal eigenvectors. Non-normality results in transient growth of disturbances for a linearly stable system. They also showed that transient growth can result in triggering, starting from a small, but finite initial condition.

Mariappan and Sujith (2010) numerically investigated the stability of a solid rocket motor. They identified and incorporated the terms contributing to the non-normality in the acoustics and propellant burn rate in their investigation. They observed that a system can be triggered with very low amplitude disturbance, when applied in an optimal direction. Subramanian and Sujith (2011) investigated role of non-normality in a premixed flame. They considered the flame dynamics also in their investigation and found that

it plays a vital role in triggering the system. Mariappan *et al.* (2011) confirmed experimentally that the eigenmodes of a horizontal Rijke tube are non-orthogonal. Further, they quantified transient growth using acoustic energy as a scalar norm, and confirmed the predictions of Balasubramanian and Sujith (2008*b*).

Following the work of Sujith and co-workers, Juniper (2011) proposed that triggering in thermoacoustics is analogous to bypass transition in turbulence. He also developed a procedure based on adjoint looping to find the lowest energy that can trigger self-sustained oscillations in a horizontal Rijke tube. He showed that the initial energy required to trigger self-sustained oscillations is much smaller than the energy of the oscillations, and is even lower than the lowest energy on the unstable periodic solution. Zhao (2012) investigated a numerical model of Rijke tube with premixed flame as a heat source. In his investigation, he found that the presence of temperature gradient in the system gives rise to non-normal nature. Kim and Hochgreb (2011) experimentally investigated triggering and transient growth of thermoacoustic oscillations in a model lean-premixed swirl stabilized gas turbine combustor. In an alternate approach, Noiray *et al.* (2008) analyzed triggering using describing functions.

Fedotov *et al.* (2002) found that a nonlinear dynamical system mimicking a laminar-to-turbulent subcritical transition system with a non-normal transient growth is sensitive to the presence of weak random perturbations. They showed that non-normality is an important factor in the amplification of noise and the susceptibility of a system to be pushed out of the basin of attraction of the stable state. This finding can have a serious bearing on stability of thermoacoustic systems as they have been shown to be non-normal in general (Balasubramanian and Sujith, 2008*a*,*b*; Nicoud *et al.*, 2007)

Waugh and Juniper (2011) conducted numerical investigations and showed that low amplitude noise can cause triggering. They constructed a stochastic stability map to highlight the probabilistic nature of the transition. Studies of hydrodynamic instability in the context of bypass transition to turbulence in pipe flow have shown that a possible route to transition occurs through a complex network of saddle points and at least one local relative attractor (Duget *et al.*, 2008). The local relative attractor has just one unstable eigenvalue; so trajectories enter its vicinity along its stable manifold, and escape along the unstable manifold.

2.4 Existing understanding and out standing issues

A large number of investigations have been performed to understand the effect of noise on the dynamics of the system. The earlier studies show that noise can play both constructive and destructive role on the output of the system depending upon the type of system, the type of interaction of noise and the parameter through which noise was added to the system. Noise can play a constructive role such as stabilizing an unstable system, recede the critical value of transition, pattern formation, enhance response of the system to external perturbations etc. On the other hand, it can play destructive roles such as triggering a system, advance the critical value of transition, induce chaos etc.

Noise induced transitions have been extensively investigated in the field of physics, biology, chemical and electrical systems. Experimental investigations have also been performed, but the system considered for investigation were of simple nature. For example most investigators considered electrical oscillators to reduce complexity; further, they were of parametric oscillator type. Very few investigated the role of noise in complex system like a laser. Thus to asses the impact of noise on a practical system like combustion system, the observations made in a simple system cannot be extended in a straight forward manner.

Though considerable amount of theoretical investigation has been performed on the effect of noise on combustion system, very few experimental investigation have been performed to asses the role of noise in the system.

2.5 Objective of the thesis

In the present thesis we are interested in understanding the role of noise in a thermoacoustic system, especially when the system is operating in the bistable zone. The investigations primarily focuses on the phenomenon of noise induced transition and the mechanism of triggering through noise. The impact of noise on the thermoacoustic oscillations is also investigated. In this context, we examine how a thermoacoustic system can be triggered by low amplitude noise. The thermoacoustic system chosen for investigation is a ducted non-premixed flame in an axisymmetric Burke-Schumann

type configuration. The fuel flow rate at the tip of the burner was perturbed randomly. This influences the system as a parametric noise. The evolution of the system under the influence of the parametric noise was investigated by constructing phase portraits. Further, the probabilistic nature of the transition is studied using basic statistical tools from design of experiments and probability theory.

CHAPTER 3

EXPERIMENTAL SETUP

3.1 Configuration

In order to understand the effect of noise on the stability of the thermoacoustic system it is desirable that the experimental setup under investigation possesses the following qualities.

- The inherent noise in the system must be low. This ensures that the deterministic state of the system can be defined with a reasonable certainty for a given control parameter.
- The system must be in thermal equilibrium with its environment. This ensures that the role of external fluctuation on the system is minimum.

The parameters in the experimental setup are chosen such that the above mentioned conditions are satisfied. The details are as follows: the thermoacoustic system chosen for investigation is a laminar ducted Burke-Schumann type non-premixed flame system, similar to the one discussed in Putnam (1971). The schematic representation of the flame configuration and the setup is shown in Fig. 3.1. A brass and a quartz tube are arranged concentric to each other to achieve the Burke-Schumann flame configuration as shown in the inset of Fig. 3.1. The dimensions of the tubes used in the experiment are provided in the Table 3.1. Fuel is supplied through the central brass tube and oxidizer is supplied through the annular space between the brass tube and quartz tube. Fuel and oxidizer diffuse, mix in the combustion zone and establishes a flame at the tip of the brass tube.

The confinement provided by the quartz tube establishes an acoustic field over the flame. The upstream of both brass and quartz tube are connected individually to plenum

Table 3.1: The dimensions of the tube used in the experiment

$Tube$	$Length$ (m)	$Outer\ diameter$ (mm)	$Thickness$ (mm)
Quartz	1	50	1.5
Brass	1.3	25	0.7

chambers to maintain an acoustically open boundary condition, and to dissipate any flow fluctuation that are initially present in the fuel and oxidizer supply line.

The location of the flame inside the quartz tube is a control parameter in the experiment and it is denoted by X_f. The flame location is measured by considering the inlet of the quartz tube as a reference. A traverse mechanism is employed to vary the relative position of flame inside the quartz tube. The traverse mechanism consists of a worm gear engaged rack and pinion mechanism to allow precise variation of X_f. The traverse mechanism has a minimum resolution of $1\ mm$. The uncertainty involved in the variation of X_f is $\pm 0.5\ mm$.

In the experiment, a mixture of Methane (CH_4) and Nitrogen (N_2) in a ratio of $1:2$ by volume is used as a fuel and pure Oxygen (O_2) is used as an oxidizer. Nitrogen is used as a diluent of the fuel. The diluent is added to the fuel to reduce the temperature of the flame which in turn reduces the soot formation. The formation of soot is undesirable in the system as it constantly changes the operating conditions in the system by soot deposition and also it hinders the instrumentation. Further the usage of Oxygen ensures the anchorage of the flame on the tip of the burner and prevents lift off during experiments. The flow rate of the reactants are controlled by the individual flow control valves and they are measured using a flow meter (rotameter). The flow rates of the reactant are presented in Table 3.2 . The uncertainty in the measurement of flow rate is $\pm 50\ ccm$. The equivalence ratio of the reactants at the entry is 1 and it has an uncertainty of 7.5%. The flow rates of the reactants are chosen such that there is sufficient heat release rate to drive thermoacoustic instability and at the same time maintaining the flow to be laminar in both brass tube and annular space. The Reynolds number of the flow inside the brass tube is $Re = 197 \pm 5$ ($< \ Re_{critical} = 2300$, White (2010)) and the Reynolds number of the flow in the annular space is $Re = 40 \pm 1$ ($< \ Re_{crititcal} = 1600$, Sheen *et al.* (1997)). $Re_{critical}$ represents the critical Reynolds number at which the flow becomes unstable

. The details of the Reynolds number calculation are discussed in detail in Appendix A. Separate N_2 flush lines are provided for emergency situations like thermal runaway.

Table 3.2: The Flow rate of the reactants used in the experiment

$reactant$	$flowrate\ (lpm)$
CH_4	1
N_2	2
O_2	2

Further non-return valves are provided in each supply lines to prevent the back flow of the reactants in the system.

A $6" -$Subwoofer $(4\,\Omega, 160W)$ is directly mounted on the plenum chamber provided for the fuel (as indicated in Fig. 3.1). The speaker is used to perturb the fuel flow rate in the system precisely. Parameters such as pressure fluctuation in the combustion zone and the heat release rate can be measured in the setup in order to study the response of the system for different operating conditions.

3.2 Instrumentation

3.2.1 Combustion chamber's acoustic pressure measurement

The acoustic pressure measurements are performed using transducers mounted on the quartz tube ($X_f = 25\ cm$) and the fuel plenum chamber. Piezoelectric pressure transducers of model $103B02$, manufactured by PCB Piezotronics were used for measurements. Pressure transducers are flush mounted to the quartz tube using a teflon adapter (Fig. 3.2). The details of the calibration of the adapter are presented in the Appendix B. The frequency response curve of the teflon adapter is shown in Fig. 3.3. The response of the adapter over the frequency range of $20 - 2000\ Hz$ is constant and it has a calibration coefficient of 0.997. The phase lag in the adapter is less than 10° which is negligible. The amplitude of the pressure fluctuation ($|P'|$) inside the quartz tube is considered a measure of the system's response.

The pressure signal generated by the transducers are first conditioned using a signal

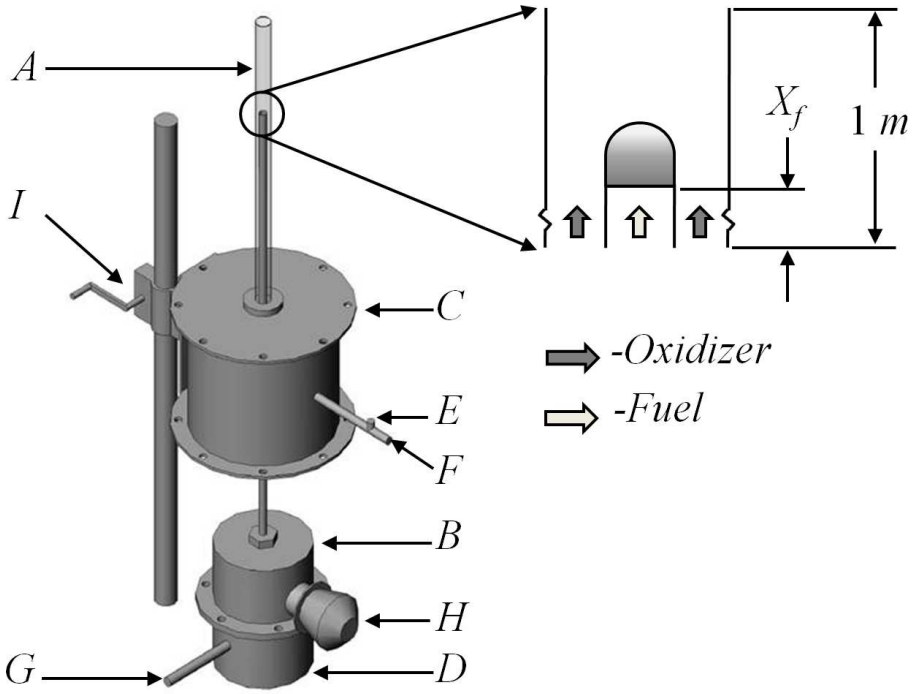

Figure 3.1: Schematic diagram of the setup. The legend represents the following: A- Quartz tube, B- Brass burner tube, C- Oxidizer plenum chamber, D- Fuel plenum chamber, E- Oxygen supply port, F- Flush Nitrogen supply, G- Fuel supply port, H- Sub woofer, I- Traverse mechanism. The inset figure represents the Burke-Schumann flame configuration.

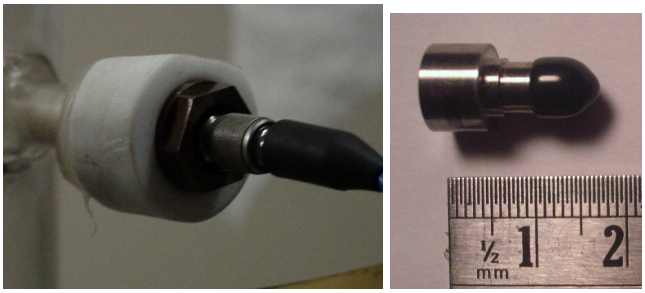

Figure 3.2: Teflon adapter used to flush mount the transducer on the quartz tube and the Piezoelectric transducer used for pressure measurements

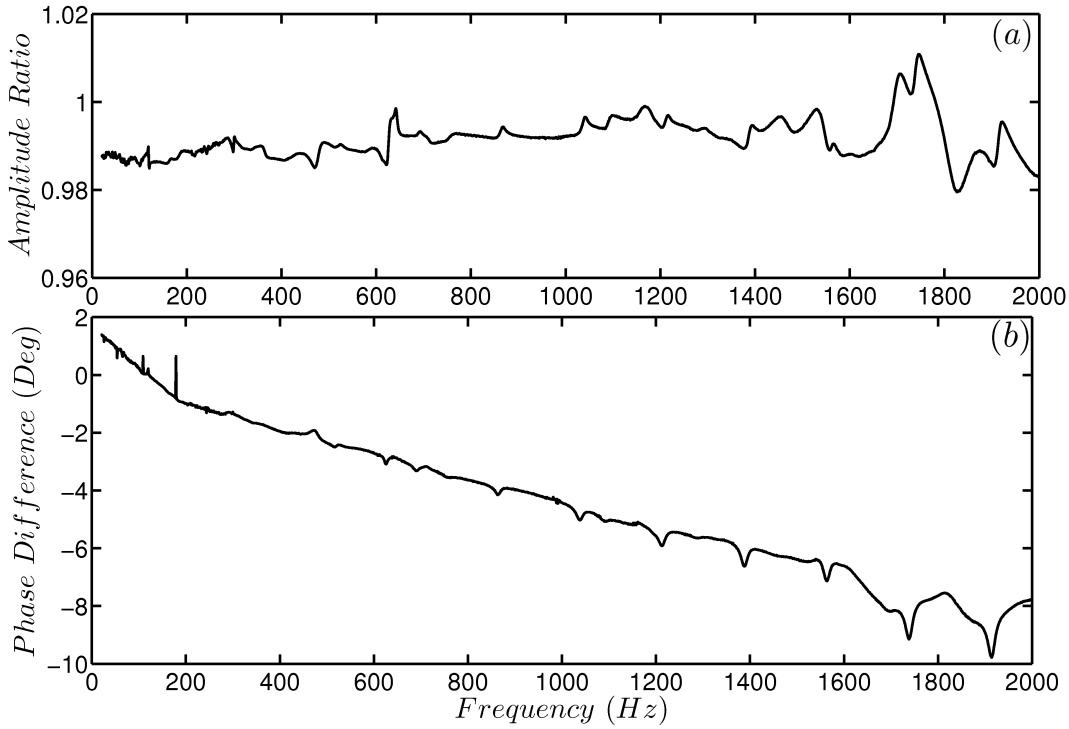

Figure 3.3: The frequency response (a) and phase difference (b) of the teflon adapter for a frequency range of $20 - 2000\ Hz$.

conditioner ($PCB\ 482A16$) and then the signal is acquired in a data acquisition (DAQ) system with $PCI\ 6221\ DAQ\ Mx$ card via a $SCB - 68$ connector card (physical interface). The acquired signal is then processed using a Labview signal express 2009. The data are acquired at a rate of 10000 samples per second. DAQ system is also used to generate the required electrical signals that has to be given to the speaker in order to perturb the system.

3.2.2 Heat release rate measurement

The spectrum emitted by the flame was first analyzed using a Aventes spectrum analyzer (Model no: $3648 - 2$) in the wave length range of $250\ nm$ to $800\ nm$. The emission spectrum of the flame is shown in Fig. 3.4 (a). The strength of the OH^* chemiluminescence signal which corresponds to the transition $OH\ A^2\Sigma^+ \rightarrow\ X^2\Pi$ (Nori and Seitzman., 2007) is measured for various fuel flow rates (equivalence ratio is maintained constant at 1). The OH^* chemiluminescence signal is observed to vary linearly with the flow rate of the fuel or the total heat release rate of the flame (Fig. 3.4 b). Hence the

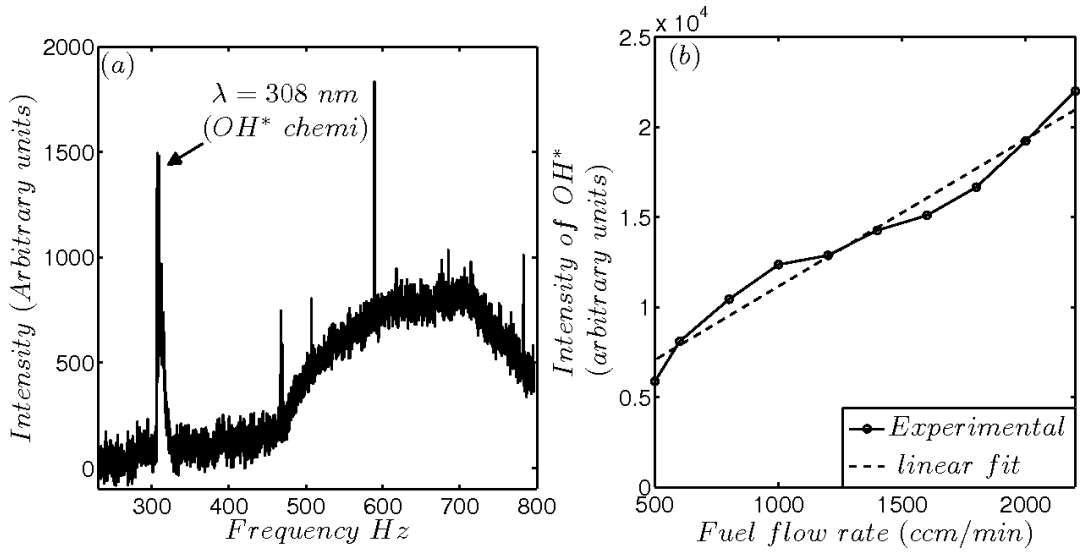

Figure 3.4: (a) Emission spectrum of the flame showing peak at $308\ nm$ wavelength. (b) Variation of intensity of OH^* signal as the mass flow rate of the fuel is increased maintaining $\phi = 1$ as constant

OH^* chemiluminescence can be used to quantify the heat release rate fluctuation of the flame (discussed in detail in Appendix C). The instantaneous fluctuation in the heat release rate of the flame is measured using a Hamamatsu $H5784$ photo multiplier tube (PMT) fitted with a $308\ nm$ narrow band filter (OH^* chemiluminescence). The wave length band of the filter is $\pm 5\ nm$. The signal generated in the PMT is collected in the DAQ system bypassing the signal conditioner. The bypassing is performed to prevent the signal conditioner from subtracting the base voltage from the PMT signal which corresponds to the mean heat release rate of the flame.

3.2.3 Temperature measurement

Thermocouples of type 'K' are mounted on the quartz tube at $X_f = 50\ cm$ to measure the wall temperature. Another 'K' type thermocouple is mounted on the control panel to measure the ambient temperature. The wall temperature of the quartz tube is measured to monitor the steady state of the system during the experiment. The ambient temperature is measured to ensure that the environmental conditions around the setup does not vary much. This is performed to ensure that environmental fluctuation have less impact on the obtained results. The relative humidity present in the air is also measured using

hygrometer to monitor the environmental changes. Experiments are always performed in an ambient temperature of $301 \pm 1\ K$ and relative humidity of $76 \pm 3\%$.

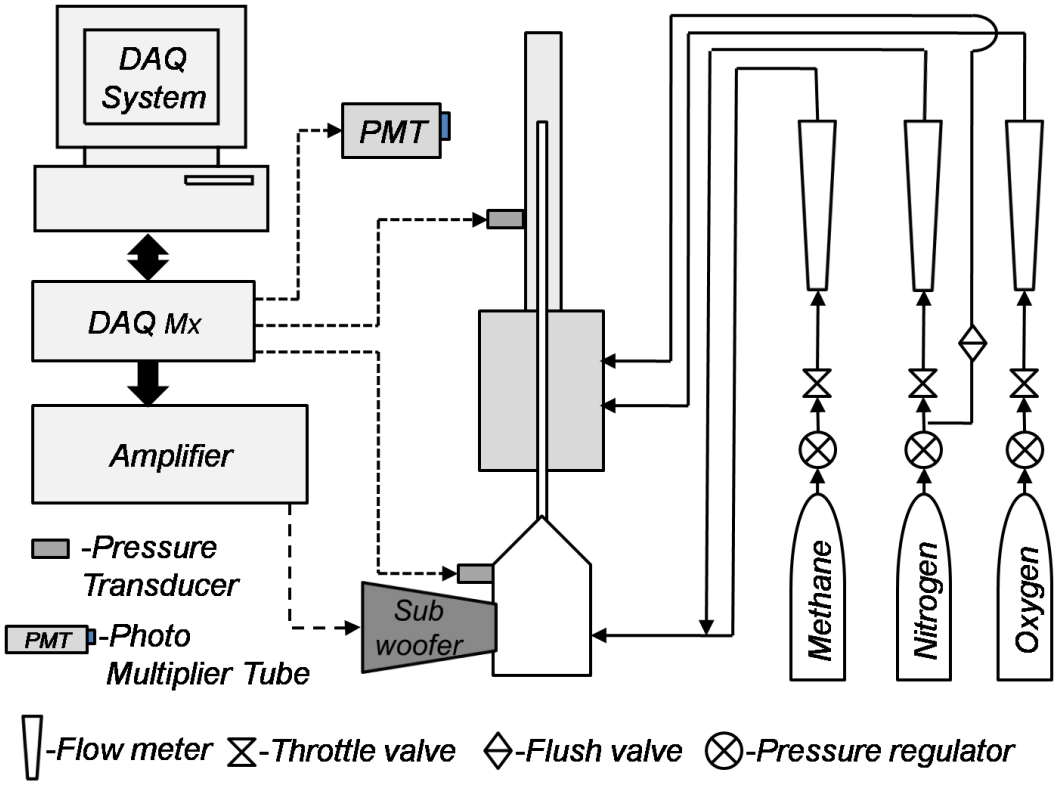

Figure 3.5: The outlay of the instrumentation, reactants control and supply of the experimental setup.

3.3 Speaker characterization

Electrical signal for the speaker are generated in the DAQ system. The generated electrical signal is then amplified in a AHUJA UBA-500M ($650\ W, Hi-fidelity$) amplifier and supplied to the speaker. The performance of the speaker is assessed to quantify the recreation of the electrical signal given to the speaker, by measuring this is quantified by measuring the total harmonic distortion (THD) of the speaker. The details of the measurement are presented in the Appendix D. The evaluation is performed for a frequency band of $1 - 1000\ Hz$ as shown in Fig. 3.6. From the Fig 3.6 we can observe that the THD is less than 5% for the frequencies above $20\ Hz$. Since the operating conditions are between $20 - 1000\ Hz$ this satisfies our requirement.

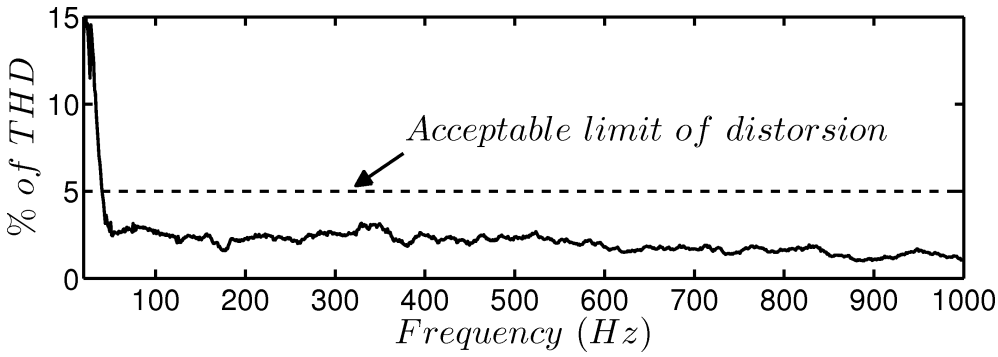

Figure 3.6: THD of the speaker for the frequency range of $1 - 1000\ Hz$.

Gaussian white noise signal is generated in the DAQ system and is supplied to the speaker. The speaker is kept in free field, and pressure measurement are acquired and processed to assess its nature. The power spectral density of the noise is shown in Fig. 3.7 (a). From Fig. 3.7 (a) we can observe that the spectrum is not perfectly flat (for a noise to be white in color the power spectral density of the noise should be flat, that is the amplitude should be same for all frequencies). Instead the spectrum shows that the amplitude increases as the frequency increases (blue noise). For a noise signal to be designated as blue in color the variation of spectral power density should be $3\ dB/octave$ with increasing frequency. The slope of the power density spectrum with increasing frequency for the noise generated by the speaker is $0.02\ dB/octave$. Hence in effect, the noise generated by the speaker can be considered as white noise. When the probability density function for the amplitude of the noise (Fig. 3.7 b) is analyzed, we can observe that it has Gaussian distribution. Thus the noise generated from the speaker is a Gaussian white noise within the frequency range $20 - 2000Hz$.

In general the power spectral density of the white noise should be flat over infinite frequency range, but in a real physical system this is not possible. But in a practical thermoacoustic system; the higher modes are weak and dormant (Waugh *et al.*, 2011), moreover the flame act as a low pass filter and the flames response to high frequency perturbations are weak (Klein, 2000). Thus as far as the flame and system is concerned, they effectively see a white noise. As per the definition of Horsethemke and Lefever (1984) noise used in the experiment can be called as Gaussian quasi-white noise (for details see Appendix D.

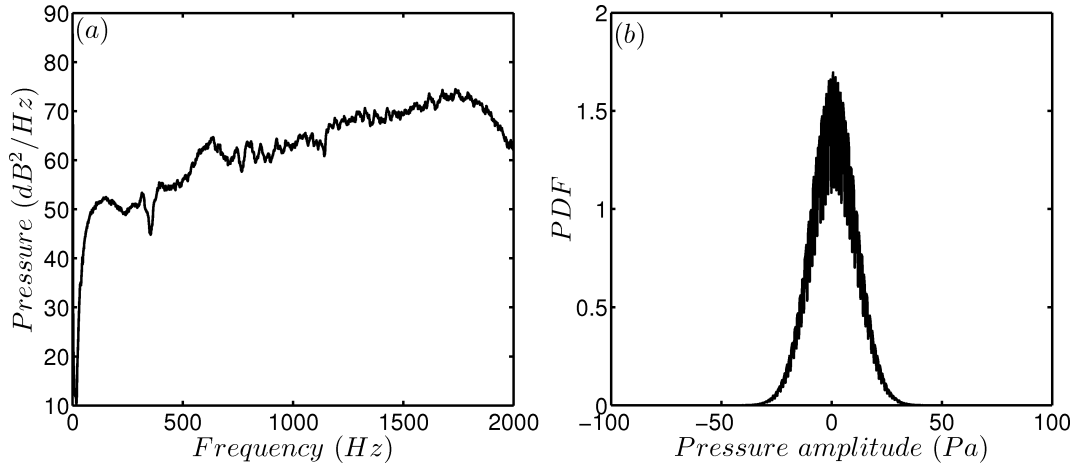

Figure 3.7: (a) Power spectral density of the white noise generated by the speaker. (b) PDF of the amplitude distribution of the noise.

3.4 Acoustic damping

In order to ensure that the system parameters does not vary between the experiments and ensure repeatability, the acoustic damping of the system represented by the decay rate (α) is measured and monitored to be within a acceptable variation limit. Damping measurements are performed at prescribed environmental conditions (see Section 3.2.3). The acoustic damping in the system is measured as prescribed by Perry (1970).

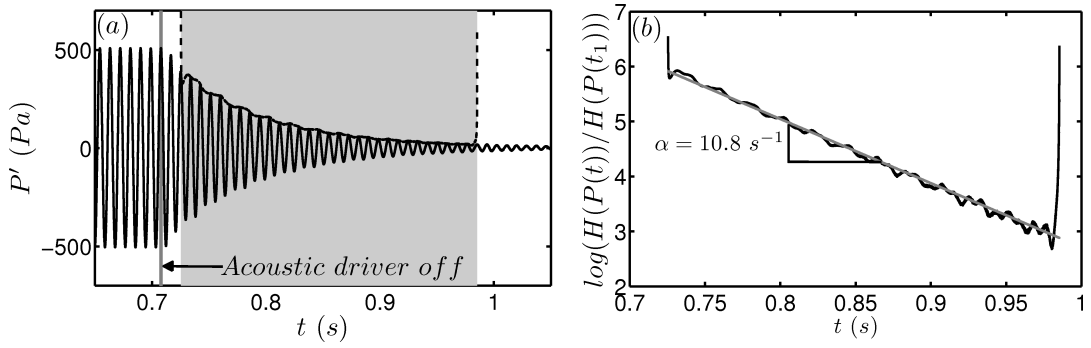

Figure 3.8: (a) The pressure trace of the system decaying to stable state (without flame). The signal within the gray shaded region is utilized to estimate the damping in the system and the dotted line represent the amplitude envelope (b) Estimation of slope of the decaying amplitude envelope.

The system is perturbed acoustically at the natural frequency of the system without flame, 113 Hz. Then the disturbance is allowed to decay and the evolution of the pressure is acquired (Fig. 3.8 (a)). From the pressure trace, the envelope of the decaying am-

plitude (shown in light grey region in Fig 3.8 (a)) is extracted by applying Hilbert transform (absolute value). The logarithmic decay rate defined by $log(|H(P(t))|/|H(P(t_1))|$ of the pressure trace is shown in Fig. 3.8 (b). The straight line part of the curve represents the exponential decay of the pressure trace. The slope of the line gives the decay rate of the system. For the case shown in Fig. 3.8 (b) the $\alpha = 10.8\ s^{-1}$. For the present study, the mean of the α is $10.6\ s^{-1}$, and the acceptable variation limit is $\pm 0.5\ s^{-1}$. The decay rate is measured before every experiment, and the experiments are conducted only if it is within the prescribed limits.

3.5 Background noise in the system

The random fluctuation or noise level in the system is quantified by the standard deviation of the fluctuations. The inherent noise present in the system was observed to be $2\ Pa$. The inherent fluctuation presented here considers both the noise associated with the DAQ system and also the inherent flow and pressure fluctuation in the system. Thus the experimental set up has very low inherent noise as stated in section 3.1.

CHAPTER 4

RESULTS AND DISCUSSION

4.1 Deterministic state of the system

The behavior of the system in the absence of noise is first investigated. The system's response ($|P'|$) for variation in control parameter (X_f) for a noise free case is represented through a bifurcation diagram. The control parameter X_f is varied in steps of $1\ mm$, and a settling time of $180\ s$ is provided for the system to reach the equilibrium state between each variation in X_f. The equilibrium state of the system is monitored through the measurement of wall temperature. $|P'|$ is measured after the system reaches the equilibrium state. $|P'|$ for variation of x_f in both forward ($X_f = 34\ cm\ to\ X_f = 31\ cm$) and return ($X_f = 31\ cm\ to\ X_f = 34\ cm$) direction is acquired.

4.1.1 Path followed by the system

The response of the system for variation of X_f is shown in Fig. 4.1. From Fig. 4.1, we can observe that the path followed by the system is not same for forward and return direction.

Assume that, the system is initially operating at point 'A'. As X_f is reduced the system continues to stay in a steady state. On reaching point 'B' the system losses stability and the amplitude of pressure fluctuation increases. The amplitude of oscillations finally reach the point 'C' and the system exhibits sustained oscillation. On further decreasing the X_f, the system continues to stay in oscillatory state and reaches point 'D'. On the return path from point 'D', the system continues to stay in the oscillatory state until it reaches the point 'C'. Even after reaching the point 'C', the system does not fall back to the stable steady state; instead the system continues to stay in oscillatory state and follows an entirely different path to 'E'. On further varying X_f, the system continues to

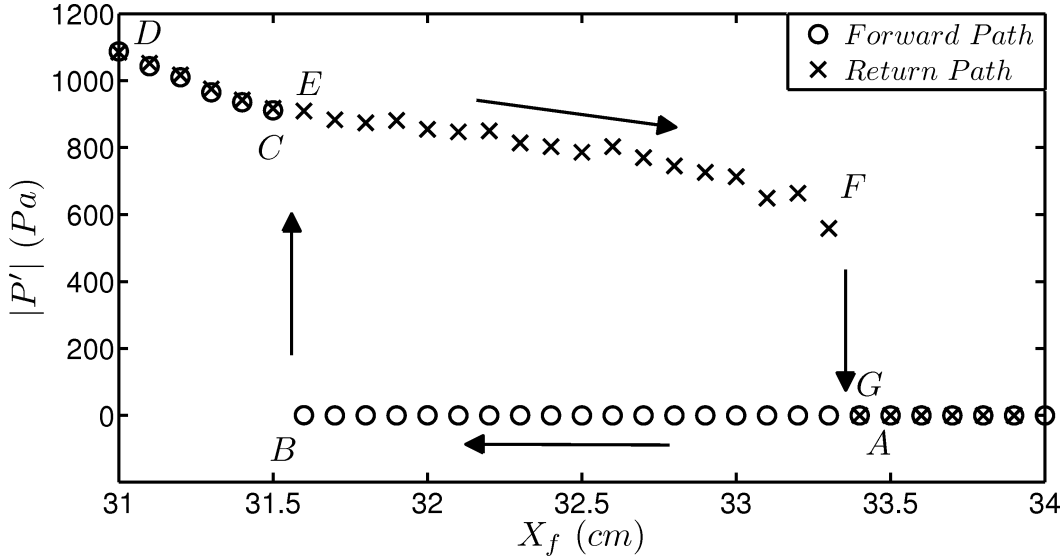

Figure 4.1: The response in P' for the variation of the control parameter X_f. The volume flow rate of $N_2 = 2\ lpm$, $CH_4 = 1\ lpm$ and $O_2 = 2\ lpm$. Settling time between each measurement is $180\ s$.

stay in the oscillatory state and reaches point 'F'. At 'F', the system is unable to sustain the oscillations and the pressure oscillations decay and it reaches the steady state and reaches point 'G'. The system continues to stay in steady state for further variation of X_f. The system is observed to exhibit 'bistability' or hysteresis between $X_f = 31.5\ cm$ to $X_f = 33.3\ cm$.

The oscillatory state attained by the system is 'limit-cycle oscillation', as can be clearly observed from the phase portrait constructed using pressure fluctuation inside the combustion chamber $P'\ (Pa)$ and fluctuating heat release rate of the system q' $(arbitrary\ units)$ (Fig. 4.2). Since the data are from experiments the limit cycle appears to be banded. The above explained experiments were performed three times to ensure repeatability.

4.1.2 Triggering phenomenon

When the system is operating in the hysteretic region the phenomenon of triggering can be observed. In Fig. 4.3 the phenomenon of triggering instability is illustrated. As prescribed by Mariappan *et al.* (2011), in the experiment the system was perturbed with an initial condition of 20 cycles of sine wave of frequency $185\ Hz$ (natural frequency

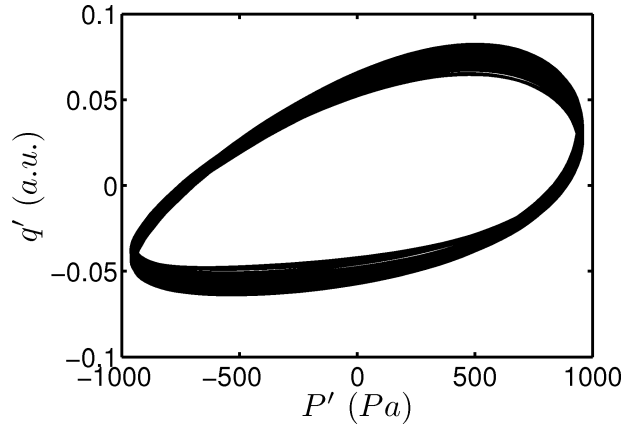

Figure 4.2: Phase portrait of the system is constructed using q' and P'. The phase portrait shows the closed trajectory, hence the nature of oscillation is limit-cycle ($X_f = 32\ cm$).

of the system with the flame). Twenty cycles of oscillation were used to perturb the system to overcome the inertia of the system to respond to a disturbance. To identify the triggering amplitude of the system, the amplitude of the disturbance is increased in steps of $2\ Pa$ and the system was perturbed and then allowed to evolve on its own. If the disturbance destabilizes the system, the amplitude of the oscillation will increase and finally reaches the stable oscillatory state as shown in Fig. 4.3 (a). The amplitude of the disturbance is then identified as the triggering amplitude. If the disturbance amplitude is less than the triggering amplitude, the disturbance decays and as this system evolves, asymptotically reaches the steady state (Fig. 4.3 (b)). The above explained experiments were performed for all X_f within the bistable region (with a step size of $1\ mm$) and the experiments were repeated twelve times to quantify the uncertainty in the triggering amplitude.

The triggering amplitude for the system depends on the type of initial condition with which it was perturbed. The triggering amplitude identified in the current experiment corresponds to initial condition specified above. For a single mode perturbation (like the one used in the experiment), the first mode requires least energy for the system to get triggered (Mariappan *et al.*, 2011).

The evolution of the heat release rate ($q(t) = \bar{q}(t) + q'(t)$) of the system is shown in Fig. 4.3 (c) & (d). In Fig. 4.3 (c), the heat release rate of the system during triggering instability is presented. The heat release rate is observed to oscillate after the distur-

bance is imparted to it. The pressure and velocity oscillation in the chamber enhances the mixing of the fuel and oxidizer and it reduces the effective local equivalence ratio in the combustion zone. This increased mixing is reflected in the OH^* intensity trace as a decreasing mean (Nori and Seitzman., 2007). The change in the local equivalence ratio leads to increase in mean heat release rate. Thus decrease of the mean of OH^* intensity indicates increase in mean heat release rate $(\bar{q})$. Along with the increase in $\bar{q}$ the amplitude of the fluctuating heat release rate (q') also increases exponentially and reaches a stable oscillatory state. The heat release rate of the system that did not got triggered is shown in Fig. 4.3 (d). Here the heat release rate is observed to oscillate but the oscillations are not sustained and they decay exponentially similar to a pressure evolution shown in Fig. 4.3 (b).

The phase difference (ϕ) between the q' and P' is measured from the time series data and is presented in Fig. 4.3 (e) and (f). The method followed to acquire the phase difference between P' trace and q' trace is as follows; first the time traces are divided into small segments of time interval of $25\ ms$: the time interval is 4.6 times longer than the acoustic timescales of the system, which is $5.4 \times 10^{-3}\ ms$ and it corresponds to the natural frequency of $185\ Hz$. Then the cross correlation coefficient between the corresponding divided time traces are acquired. Finally the $\arccos$ $(\cos^{-1})$ of the correlation coefficient gives us the phase difference between the traces.

The evolution of ϕ for the system that just got triggered is shown in Fig. 4.3 (e). When the system is in steady state, q' and P' are out of phase (90°). When the disturbance is imparted, ϕ evolves and establishes a strong coupling to overcome the threshold. After the threshold is exceeded ϕ evolves such that the coupling between q' and P' weakens and it is just sufficient enough to overcome the damping in the system and to sustain the oscillation. The evolution of ϕ for the system that is not triggered is presented in Fig. 4.3 (f). As explained earlier the q' and P' are initially out of phase, when perturbed the ϕ evolves but it is unable to establish a strong coupling to overcome the threshold, thus the ϕ drifts back and again reaches the state where it is out of phase.

The phase portrait of the system that just got triggered is shown in Fig. 4.3 (g). Initially the system is in steady state (fixed point), when a disturbance is imparted to the system it spirals out and reaches the unstable limit cycle, shown as a dark band. The

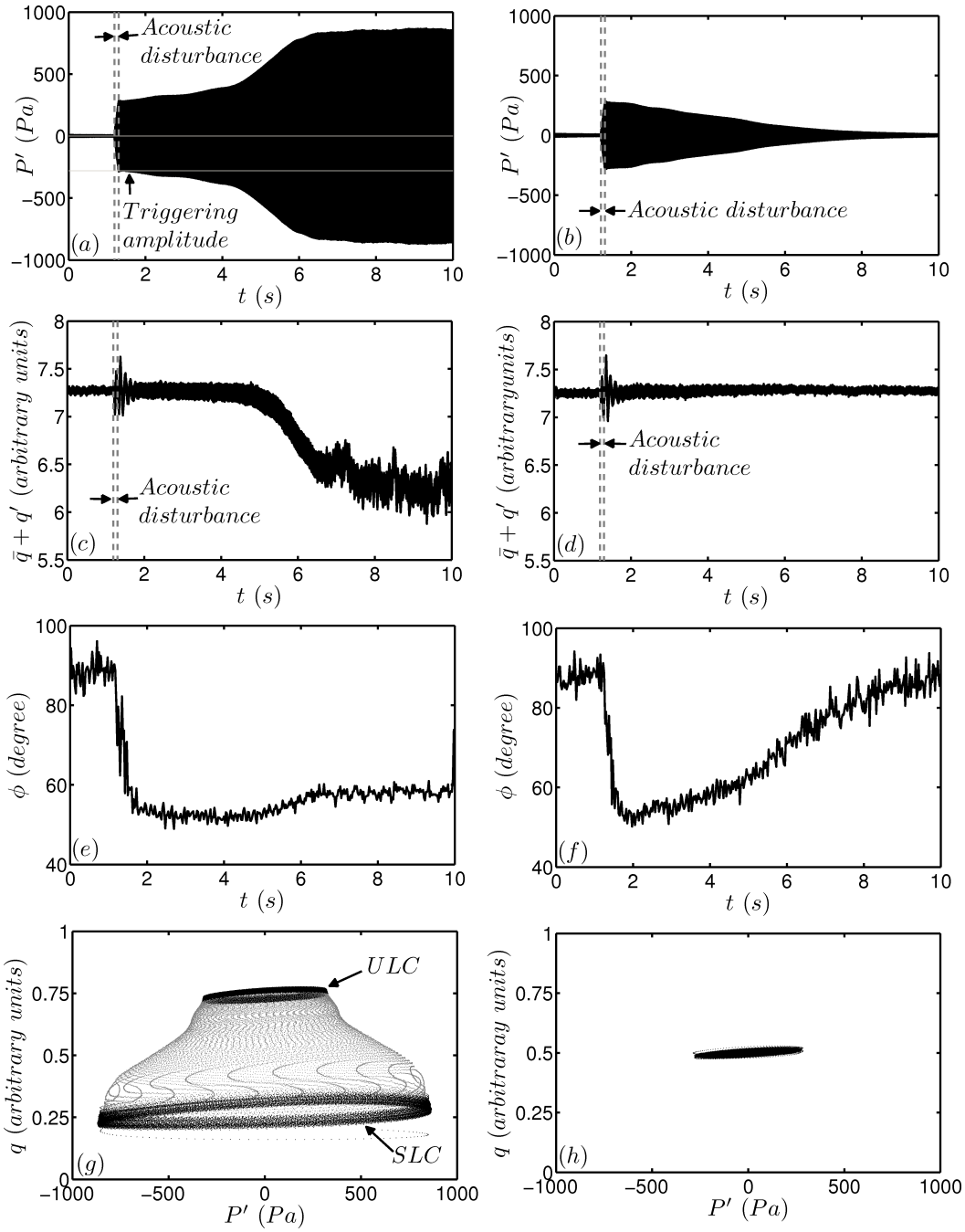

Figure 4.3: The evolution of the system at $X_f = 32.3\ cm$, after it was perturbed is represented in pressure (a) & (b), heat release rate (c) & (d), phase difference (e) & (f) and phase portrait (g) & (h) of the system. The figures (a), (c), (e) & (g) corresponds to the system that just got triggered. The amplitude of the initial disturbance is $289\ Pa$. The figures (b), (d), (f) & (h) corresponds to the system not getting triggered and asymptotically reaching steady state. the amplitude of the initial disturbance is $279\ Pa$. At $X_f = 32.3\ cm$ the triggering amplitude is $284\ Pa$ with an uncertainty of $\pm 2\ Pa$. The term ULC denotes Unstable limit-cycle and the term SLC denotes Stable limit-cycle. The time intervals chosen for calculation of ϕ is $0.025\ s$. The scales of the plots are maintained same for plots of both triggered and un-triggered case.

unstable limit-cycle represents the threshold, the system has to overcome in order to get triggered. For the present case, the amplitude of the disturbance is just sufficient enough to reach the threshold. After reaching the unstable limit-cycle, the system evolves in this orbit for a while before it spirals out and reaches a stable limit-cycle oscillation. Similarly the phase portrait shown in Fig. 4.3 (h) is of the system that did not get triggered. Here the disturbance takes the system to the unstable limit-cycle but the amplitude of the disturbance is not sufficient enough to cause triggering. The system hovers in this orbit for a while before it decays down to the steady state. In the phase portrait we are unable to clearly define the mean heat release rate of the system, hence from Section 4.1.3 onwards we will only consider the evolution of fluctuating heat release rate (q') of the system. The evolution of the mean heat release rate of the system will be removed from the time trace by passing it through a high pass filter which has a cut-off frequency of $5\ Hz$ (Bendat and Piersol, 1986).

These observations fit the conjecture proposed by Juniper (2011) that when the system is just triggered, the oscillations transiently grow towards an unstable periodic orbit before growing to a stable periodic orbit. The oscillatory limit cycle state and the fixed point state are separated by a basin boundary. The unstable limit cycle lies on the surface of the basin boundary (Duget *et al.*, 2008). If the initial perturbations take the system across the basin of attraction, the system evolves to a self-sustained oscillatory state. If the initial conditions falls within the basin of attraction of a stable fixed point, the oscillations decay to the fixed point.

4.1.3 Consolidated stability map

A consolidated bifurcation diagram is presented in Fig. 4.4. The points denoted by the upward triangle represents the oscillatory state of the system. The points denoted by the downward triangle represents the steady state of the system. The dotted line represents the triggering amplitude of the system. The error bar on the triggering amplitude represents the maximum and minimum value of the triggering amplitude obtained from realizations and the dotted line passes through the mean of the values obtained for the particular X_f. The system becomes unstable at $X_f = 31.45 \pm 0.05cm$ and the flame

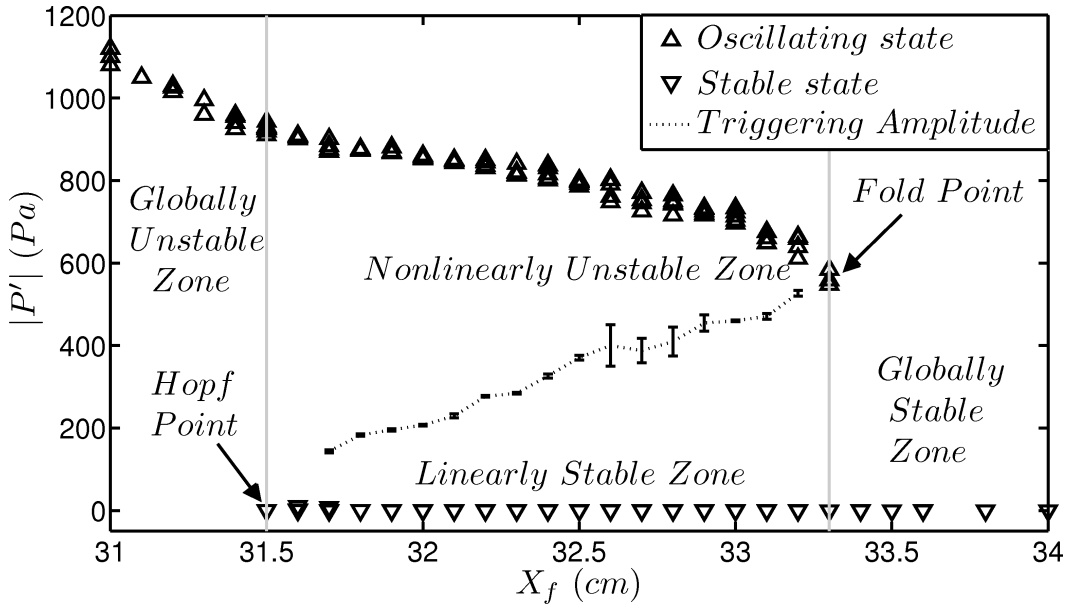

Figure 4.4: Consolidated bifurcation diagram of the system. The region between $X_f = 31.5\ cm$ to $X_f = 33.3\ cm$ the system is bistable. The error bar on the dotted line represents the uncertainty associated with the identification of the triggering amplitude.

location is called as Hopf point. The system becomes stable at $X_f = 33.25 \pm 0.05cm$ and the flame location is called as fold point.

On observing the bifurcation diagram the stability of the system can be classified into three zones. The operating conditions above the Fold point ($> X_f = 33.25\ cm$) is said to be non-linearly stable or globally stable. When the system is operating in the globally stable region, any disturbance imparted to the system will eventually decay and reach a steady state irrespective of the amplitude of the disturbance. The X_f below the Hopf point ($< X_f = 31.45\ cm$) is said to be linearly unstable or globally unstable. when the system is operating in globally unstable region, even an infinitesimally small disturbance such as the inherent noise present will destabilize the system and will reach the oscillatory state. The region between the Hopf point and the fold point is called as the bistable zone or the subcritical transition zone as the system undergoes transition to instability via subcritical Hopf bifurcation. In the subcritical transition zone, the system is stable as long as the amplitude of disturbance is less than the triggering amplitude. The system will become unstable and reach a oscillatory state if the amplitude of the disturbance is greater than the triggering amplitude.

Since the deterministic behavior of the system is clearly defined, the flame locations $X_f = 32\ cm,\ 32.2\ cm,\ 32.4\ cm,\ 32.6\ cm,\ 32.8\ cm$ and $33\ cm$ are chosen for the noise induced triggering experiment. The triggering amplitudes for the corresponding flame location in presented in Table 4.1.

Table 4.1: Triggering amplitudes for the flame locations chosen for noise induced triggering experiments

$X_f\ (cm)$	$Triggering\ amplitude\ (Pa)$
32	207.0
32.2	277.0
32.4	326.3
32.6	400.0
32.8	409.4
33	460.0

4.2 Noise induced triggering and its stochastic nature

To understand the effect of noise on the stability of the system and the stochastic nature of the occurrence of transition, a systematic and controlled experimental study was performed. The experimental parameter in our current study is the strength of noise with which the system is perturbed. Noise is added to the system through the speaker mounted on the fuel plenum chamber. Perturbing the system with Gaussian quasi-white noise reflects in the system as a fuel flow rate fluctuation. Since the heat release rate of the system is almost linearly related to fuel flow rate (see Section 3.2), fluctuating the fuel flow rate randomly leads to randomly fluctuating heat release rate, which is equivalent to a parametric noise. As a first step, we quantify the fuel flow rate fluctuation and the nature of the fluctuation at the tip of the burner by performing velocity measurements using high speed particle image velocimetry (HS-PIV) and laser doppler velocimetry (LDV) in cold flow state. The details of the velocity measurements are explained in detail in Appendix E. Then an experiment was specifically designed to capture the stochastic nature of the occurrence of NIT. In the experiment, the evolution of the P' and q' under the influence of the noise is acquired. From the acquired pressure, heat release rate data and the final state reached by the system, the stochastic properties

of the system is quantified. The time duration of the experiment for which the evolution is captured was chosen as $90\ s$.

4.2.1 Fuel flow rate fluctuation

The velocity measurement was first performed for a noise free case. The velocity profile at the tip of the burner is shown in Fig. 4.5. The velocity profile at the exit of the burner tube was observed to be almost parabolic in nature, similar to a profile of a fully developed Hagen-Poiseuille flow (O'Neill *et al.*, 2004; Rankin *et al.*, 1983). The spatio-temporal averaged velocity at the tip of the burner is found to be $\bar{V}_{avg} = 0.122\ m/s$ and the temporally averaged maximum velocity observed in the profile is $\bar{V}_{max} = 0.221\ m/s$ (the quantities denoted by bar sign $(\bar{})$ represents the temporally averaged data, the quantities denoted by 'avg' in the subscript $(_{avg})$ represents the spatially averaged data and the quantities with prime $(')$ represent the time evolving fluctuating component of the system). The temporal evolution of V_{max} was observed to have an inherent fluctuation (V'_{max}) of less than $1\%\ of\ \bar{V}_{max}$, this ensures that the flow is laminar (Darbyshire and Mullin, 1995; Crow and Champagne, 1971). Since the volume flow rate $(\dot{Q})$ at the tip of the burner is directly proportional to the V_{avg} (spatially averaged velocity across the burner, see Appendix E), the evolution of the V_{avg} is used to define the volume flow rate fluctuation in the system.

The system was perturbed by a Gaussian quasi-white noise and the fuel flow rate fluctuation at the tip of the burner was acquired. The evolution of the pressure inside plenum chamber and velocity fluctuation at the tip of the burner are shown in Fig. 4.6 (a) and (b) respectively. The spectrum of the acquired velocity data is shown in Fig. 4.7. Though the noise added to the system is white in nature, the spectrum of the velocity fluctuation shows distinct peaks at discrete frequencies. These distinct peaks corresponds to the natural frequency of burner tube assembly. The fluctuations in the noise corresponding to the natural frequency of the burner tube assembly gets amplified due to the acoustic field and they change the profile of the noise added to the system. However the distribution of the amplitude is still Gaussian in nature. Hence the profile of the noise can be still considered as "Gaussian quasi-white noise" but with

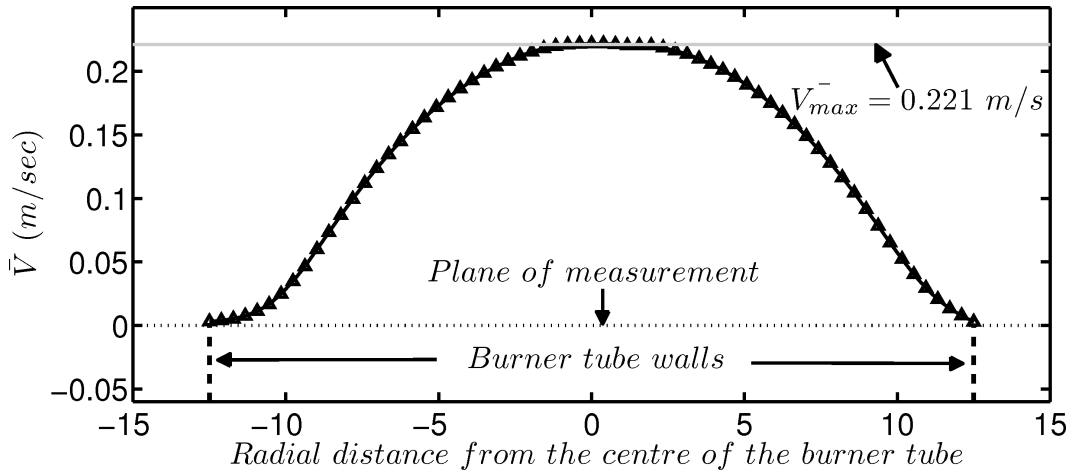

Figure 4.5: The velocity profile at the exit of the burner tube for the fuel flow rate mentioned in Table 3.2. The dashed lines represents the location of the walls of the burner. The dotted lines represent the plane of measurement which is $2\ mm$ from the tip of the burner.

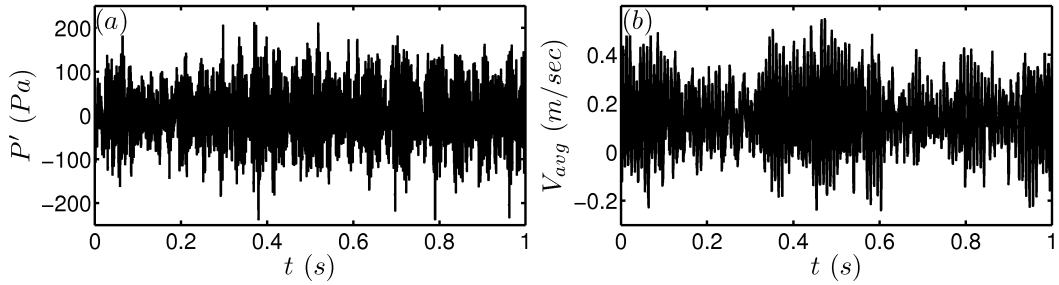

Figure 4.6: (a) Pressure trace observed in the fuel plenum chamber. (b) The V_{avg} observed at the tip of the burner.

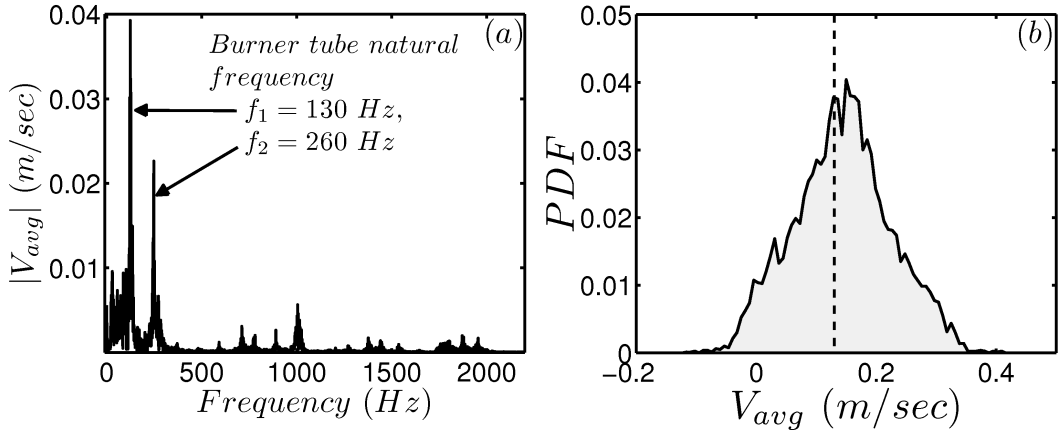

Figure 4.7: (a) Spectrum of V'_{avg} at the tip of the burner tube when perturbed with noise. (b) Distribution of the amplitude of velocity fluctuation.

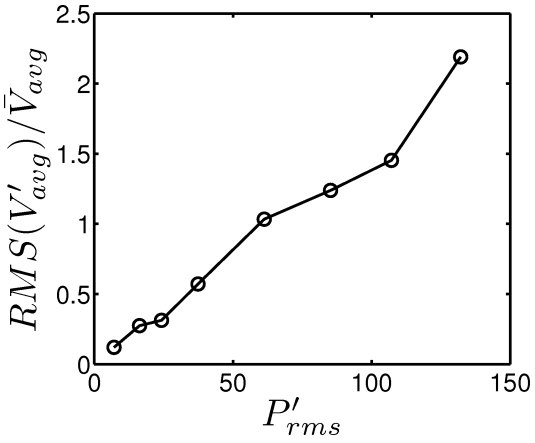

Figure 4.8: Transfer function constructed between P'_{rms} and $RMS(V'_{avg})$

contamination at discrete frequencies. As explained in Section 3.5 the noise level is quantified by the standard deviation of the pressure fluctuation. A transfer function was constructed between the noise level inside the fuel plenum chamber $(P'_{rms(pc)})$ and the fluctuating average velocity (V'_{avg}) observed at the tip of the burner and it is shown in Fig. 4.8.

Table 4.2: The noise levels used in the experiment to perturb the system. $P'_{rms(pc)}$- RMS of pressure fluctuations measured in the the fuel plenum chamber, P'_{rms}- RMS of pressure fluctuation (noise level) measured in combustion chamber at $X_f = 33.5\ cm$, RMS(V_{avg})- The RMS of the spatially averaged velocity fluctuations, RMS(q')- The RMS of the heat release rate fluctuation at $X_f = 33.5\ cm$.

$P'_{rms(pc)}\ (Pa)$	$P'_{rms}\ (Pa)$	$RMS(V'_{avg})\ (m/s)$	$RMS(q')\ (\%)$
25	18.6	0.04	1.4
49.1	38.8	0.10	3.2
73.9	57.2	0.14	7.4
98.5	100	0.17	14.5

4.2.2 Experimental parameter

Four noise levels were chosen for investigation, under which the system was observed to evolve. The noise levels are presented in Table 4.2. The corresponding fuel flow rate fluctuation at the tip of the burner and the equivalent heat release rate fluctuation are also presented in the table. The values presented in the Table 4.2 were acquired when

the system was operating at $X_f = 33.5\ cm$. The PDF of the amplitude distribution of the noise levels are presented in the Fig. 4.9.

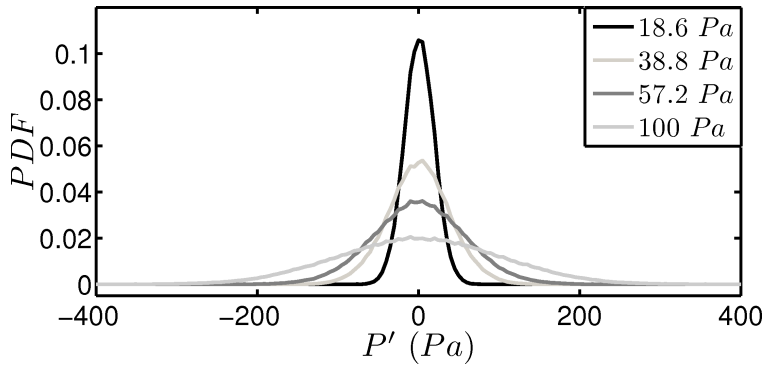

Figure 4.9: Distribution of pressure fluctuation measured inside the combustion chamber for various noise level. Measurements are acquired at $X_f = 33.5\ cm$.

4.2.3 Test of significance

To ensure the stationarity of the obtained statistical quantities, optimal number of experiments have to be performed. To identify the optimal number of experiments, a convergence study was performed between probability for transition and the number of experiments. The probability for transition is a stochastic property of the system, which will be explained in detail in Section 4.2.4. The convergence study was performed at $X_f = 32.6\ cm$ for a noise level of $57.2\ Pa$. The result of the convergence study are presented in Fig. 4.10 (a). The probability for transition data is observed to converge with an error of $\pm 2.5\%$ for 30 number of experiments. Similar convergence study was also performed on another stochastic property of the system, the PDF for the stability of the system (for details see Section 4.2.7). The results are shown in Fig. 4.10 (b). We observe that the computed PDF converges after 25 number of experiments. Though the convergence study shows that 30 number of experiments is sufficient to ensure the stationarity, as a conservative choice we perform 40 number of experiments. Thus for a given noise level and X_f we conduct 40 number of experiments and the stochastic properties are computed from the obtained data.

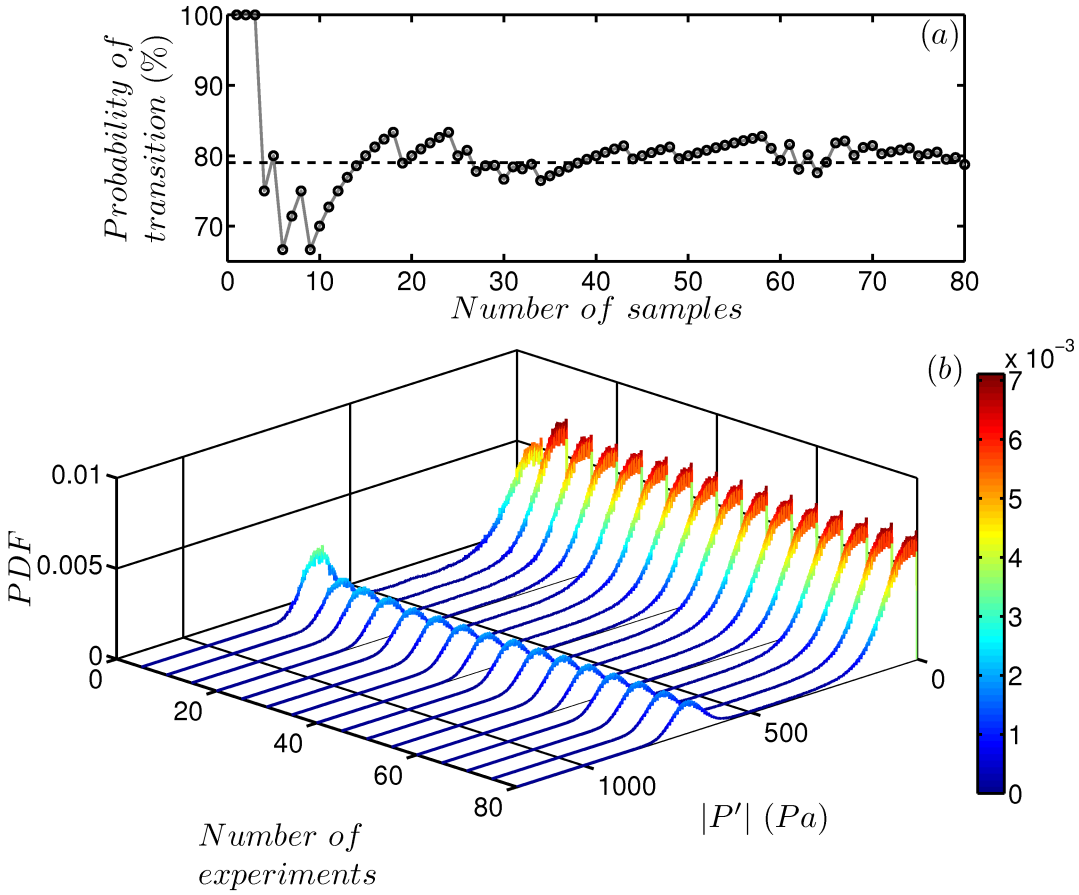

Figure 4.10: (a) Convergence of the probability for transition with number of experiments. (b) Convergence of PDF of stability of the system with number of experiments. The parameters are $X_f = 32.6\ cm$, and noise level of $57.2\ Pa$.

4.2.4 Probability for transition

Out of the 40 number of experiments conducted, the number of times the system gets triggered under the influence of noise is represented by "probability for transition". The evolution of the amplitude of pressure fluctuations inside the system is monitored continuously, if the amplitude of the pressure fluctuations increases beyond 1.2 times of the triggering amplitude of the system, then the system is declared to be triggered. Data for probability for transition are presented in Fig. 4.11. For a noise level of $18.6\ Pa$, the system does not experiences any transition for all the X_f which are considered for investigation. As the noise level is increased to $38.8\ Pa$, the system looses stability and begins to undergo transition. The probability for the system to undergo transition increases as the operating condition approaches the deterministic Hopf point. On further increasing the noise level to $57.2\ Pa$ and subsequently to $100\ Pa$ the probability for the system to get triggered also increases even as the operating conditions are receded away from the deterministic Hopf point.

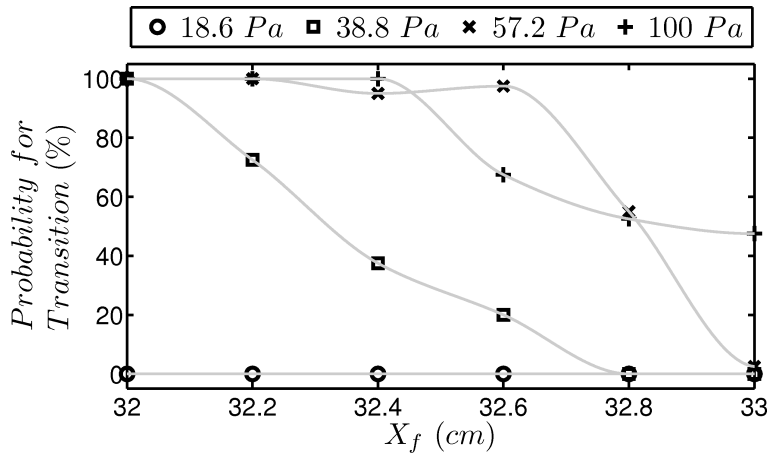

Figure 4.11: Variation of probability for transition with X_f for different noise levels

4.2.5 Average transition time

The average time taken for the transition to occur in the system is represented by the average transition time. The time instant at which the amplitude of the pressure fluctuation increases beyond 1.2 times the triggering amplitude, the system is identified as

triggered and the time period is considered as transition time. The transition time out of the 40 experiments are recorded and averaged to obtain the average transition time.

The variation of average transition time with respect to the X_f is shown in Fig. 4.12. For the noise level of $18.6\ Pa$, the system has to wait more than $90\ s$ to experience triggering. When the noise is increased to $38.8\ Pa$ the transition time becomes finite, as the system begins to experience NIT. As the noise level is further increased to $57.2\ Pa$ and $100\ Pa$, the average transition time is observed to decrease for a given operating condition. Similarly the average transition time for the system to get triggered is observed to increase as the operating condition recedes away from the deterministic Hopf point. An important feature is observed at $X_f = 32\ cm$; at this X_f the probability for the system to undergo transition is 100% for noise levels $38.8\ Pa,\ 57.2\ Pa$ and $100\ Pa$. The average transition time seems to have attained a minimum transition time for all noise level. The noise level in the system does not have any impact on the transition time. This can also be observed for flame location $X_f = 32.2\ cm$ and $32.4\ cm$ and noise level of $57.2\ Pa$ and $100\ Pa$, as the probability for transition is 100%.

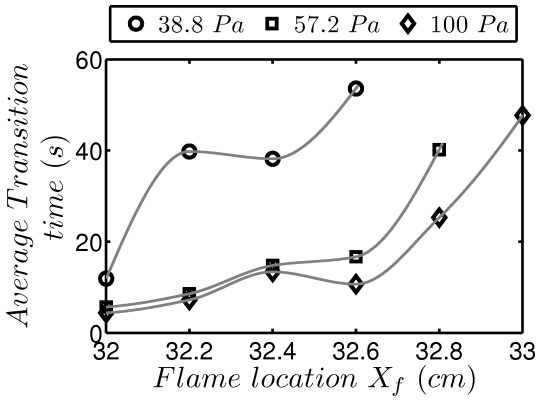

Figure 4.12: Variation of average transition time with X_f for different noise levels

4.2.6 Nature of transition

The nature of transition of the system to oscillatory state depends upon the noise level and X_f at which the system is operating. Depending upon the noise level, the system passes through certain stages before it reaches the oscillatory state. First consider the evolution of the system for a noise level of $18.6\ Pa$. In Fig. 4.13 (a) the evolution of

pressure and in Fig. 4.13 (b) the evolution of heat release rate is shown. In the pressure trace we can observe sudden spurts in the amplitude of oscillation. The occurrence of these sudden spurts becomes more prominent as the operating conditions approach the deterministic Hopf point. On further analyzing the pressure trace and heat release rate evolution, the phase difference between P' and q' evolves such that the coupling becomes stronger momentarily (see Fig. 4.13 c).

A non-dimensional quantity Γ is defined as in the Eqn. 4.2. This measures the evolution of difference in acoustic driving of the system in comparison to the driving observed at $t = 0$. Since the acoustic driving is defined for a time period, for the present investigation we choose a time interval of $0.1\ s$. The time interval is chosen such that it is equivalent to 2 acoustic time periods of $20\ Hz$ oscillations (lowest frequency of oscillation encountered in the present investigation) and 18.5 acoustic time periods of $185\ Hz$ (first natural frequency of the system).

$$\gamma(t) = \int_{t}^{t+\Delta t} P'.q'dt \tag{4.1}$$

$$\Gamma(t) = \frac{\gamma(t) - \gamma(0)}{\gamma(0)} \tag{4.2}$$

where Δt is the time interval and it is $0.1\ s$
t represents the time instant at which the Γ is measured
$\gamma(0)$ represents the acoustic driving observed in the system in the time interval $t = 0$ and $t + \Delta t = 0.1\ s$.

The evolution of Γ is shown in Fig. 4.13 (d). We are able to observe that the occurrence of spurts and transient increase in acoustic driving of the system by several orders of magnitude occur at the same time. The increase in driving can be considered as an indirect indicator of increase in energy of the system. The sudden increase in driving could be due to non-normal nature of the thermoacoustic system (Balasubramanian and Sujith, 2008*a*,*b*; Mariappan *et al.*, 2011; Kim and Hochgreb, 2011).

The other possible explanation for the formation of spurt is that, the fluctuation in fuel flow rate could fluctuate the local equivalence ratio in the system. The fluctuation

in the equivalence ratio could sometime take the system to a limit where the stable fixed point could momentarily change to unstable fixed point. This momentary change can cause a temporary growth in the amplitude of fluctuation. This is more likely to occur as the operating condition approach the Hopf point. At present the transient growth of energy is well below the threshold of triggering, hence the system did not undergo NIT. It is observed that the system always exhibits spurt formation just moments before it is about to undergo transition.

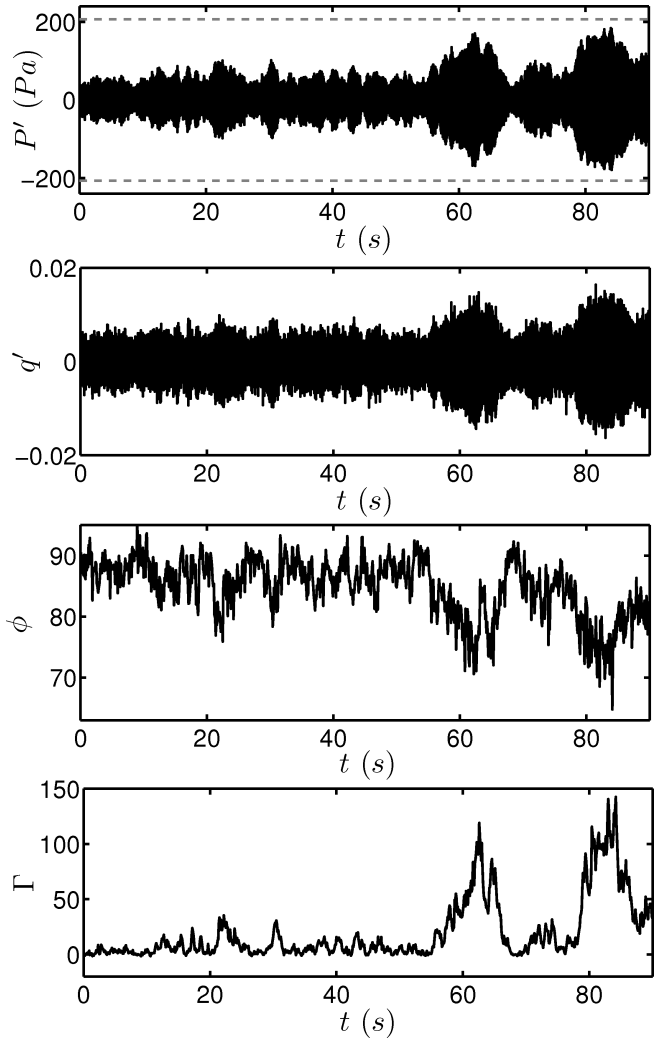

Figure 4.13: The evolution of acoustic pressure (a), heat release rate (b), phase difference (c) and driving (d) for noise level of $18.6\ Pa$, at $X_f = 32\ cm$. The dotted lines represent the triggering amplitude of the deterministic system.

As the noise level is increased to $38.8\ Pa$, the system experiences NIT and reaches an oscillatory state (limit-cycle oscillation). The nature of transition at various X_f and for a noise level of $38.8\ Pa$ are illustrated in the time histories and phase portraits

shown in Fig. 4.14. At $X_f = 32.4\ cm$ (Fig. 4.14 a and b), the deterministic triggering amplitude is 8 times larger than the noise level. First the system exhibits spurts in the amplitude of oscillation. The spurts tries to take the energy level in the system close to the threshold of triggering but is unable to do so. The system then experiences a sudden increase in the amplitude of oscillation and the energy levels in the system have now reached the triggering threshold (marked as ULC in Fig. 4.14 (c)). The system loops around this state for a brief period of time, and from this intermediate state the system spirals out and reach the stable limit-cycle orbit. This shows the system undergoes transition to instability through bypass transition, as it was predicted by Waugh *et al.* (2011) and Waugh and Juniper (2011).

Triggering amplitude depends on the proximity to the Hopf point; it decreases as we approach the Hopf point, as is seen in Fig. 4.4. Therefore, the triggering amplitude at $X_f = 32.2\ cm$ will be smaller than that at $X_f = 32.4\ cm$. At $X_f = 32.2\ cm$ (Fig. 4.14 d and e) the system first exhibits spurts in the amplitude of pressure and heat release rate trace, and noise takes the system to amplitudes levels equivalent to the triggering amplitude. Though the amplitude level have reached levels equivalent to the triggering amplitude of the system, the system does not become unstable and does not reach the oscillatory state immediately. As explained in Section 4.1.2, the triggering amplitude of the system depends on the type of initial condition (Mariappan *et al.*, 2010). The triggering amplitude of a thermoacoustic system is not only a function of amplitude of the disturbance, but it also depends on various other factors like phase relation between heat release and pressure oscillation, flame shape, distribution of energy etc., (Juniper, 2011). The system reaches the threshold limit several times and waits for a conditions when the above mentioned factors are in favor of undergoing transition. Once this favorable condition is attained, the system exceeds the triggering amplitude threshold and reaches the limit-cycle oscillation.

At $X_f = 32\ cm$ (Fig. 4.14 g and h) the noise level in the system is $1/4$ of the triggering amplitude of the deterministic state. The noise helps the system to cross the triggering threshold to reach the basin of attraction of the limit-cycle orbit. From this state, the system undergoes transition and reaches the limit-cycle orbit directly. From the pressure trace shown in Fig 4.14, we can observe that the transition time reduces as

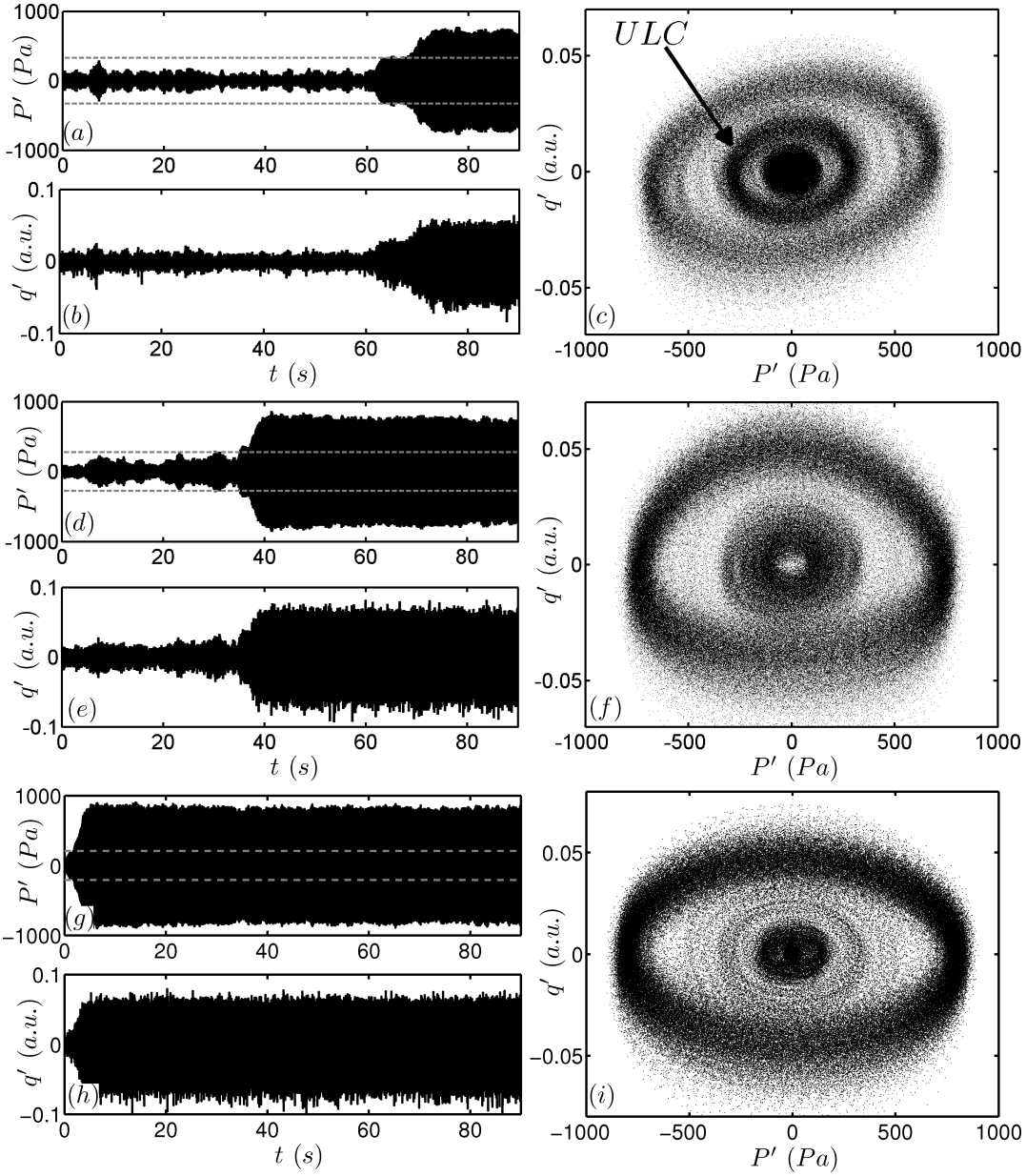

Figure 4.14: The evolution of acoustic pressure and the corresponding phase portraits for noise level of 38.8 Pa at $X_f = 32.4\ cm$ (a-c), $X_f = 32.2\ cm$ (d-f) and $X_f = 32\ cm$ (g-i). The phase portrait is constructed using P' and q' data. The dotted line on the pressure trace represent the deterministic triggering amplitude of the system. The term 'ULC' in (c) represents the unstable limit-cycle state of the system.

the operating conditions approach the Hopf point, as explained in Section 4.2.5.

In Fig. 4.15 the nature of transition of the system at $X_f = 32.6\ cm$ for various noise levels are shown. When compared to the deterministic triggering amplitude at $X_f = 32.6\ cm$ $(403\ Pa)$, the noise level of $38.8\ Pa$ is only $1/10^{th}$; however, the noise level is still able to trigger the system. This can be observed in Fig. 4.15 (a-c). Under the influence of noise, the system experiences transient growth in acoustic energy and also it aides the system to add energy in the optimal direction of maximum amplification (Juniper, 2011). Once sufficient energy is being added in this optimal direction, it causes a spontaneous increase in the amplitude of the system. Similar to the case shown in Fig. 4.14 (a), the system first reaches the intermediate triggering threshold (Fig. 4.15 c, see the dark intermediate state marked ULC) and the system evolves around this state for a while and from this state the system eventually spirals out to a stable limit-cycle orbit.

On further increasing the noise level to $57.2\ Pa$, the system exhibits a very unique phenomenon. The noise level is not only strong enough to take the system towards oscillatory state, but also strong enough to bring it back towards steady state. This causes the system to switch between the steady state and the limit-cycle orbit. The phenomenon of the thermoacoustic system switching between the two states is shown in Fig. 4.15 (c) (and also in Fig. 4.16 a). The evolution of the phase difference between the q' and P' (see Fig. 4.16) was investigated during the occurrence of the phenomenon. We observe that P' and q' are in phase when the system is in oscillatory state and out of phase when the system it is in steady state. The noise interferes with the coupling between P' and q' thus causing the system to switch between the two states. In the phase portrait (Fig. 4.15 f) we could observe these two states distinctly. Further increasing the noise level to $100\ Pa$, the system still exhibits the phenomenon of switching but the frequency of the system switching between the states has been observed to increase.

4.2.7 Stochastic stability map

Practical combustion systems are inherently noisy. Therefore, linear stability margin in a bistable region can be misleading. Thus, to analyze the "practical stability" of a system, we construct a stochastic stability map following Waugh and Juniper (2011).

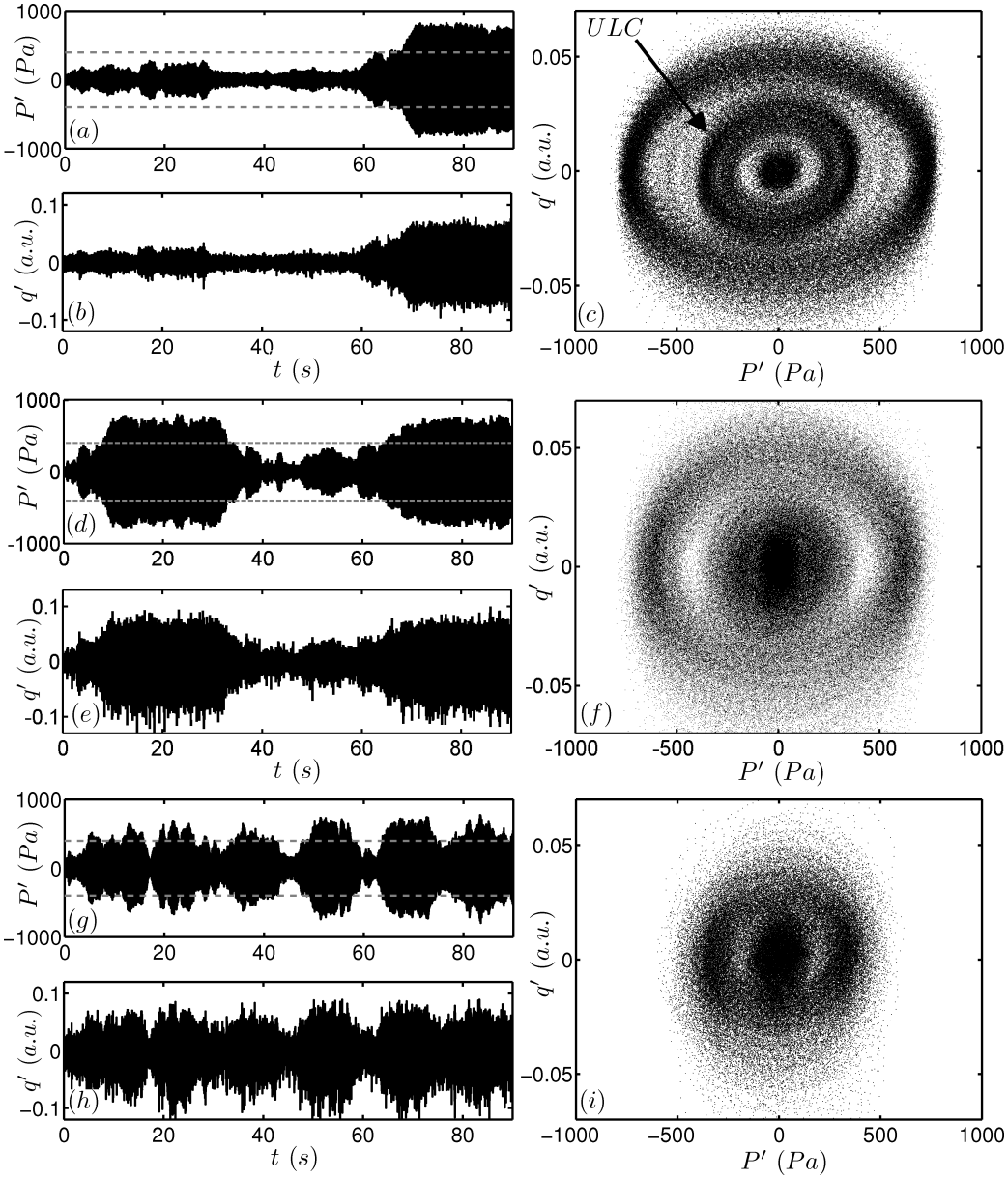

Figure 4.15: The evolution of acoustic pressure, heat release rate and the corresponding phase portraits at $X_f = 32.6\ cm$ for noise levels of $38.8\ Pa$ (a-c), $57.2\ Pa$ (d-f) and $100\ Pa$ (g-i). The phase portrait is constructed using P' and q' data. The term 'ULC' in (c) represents the unstable limit-cycle state of the system.

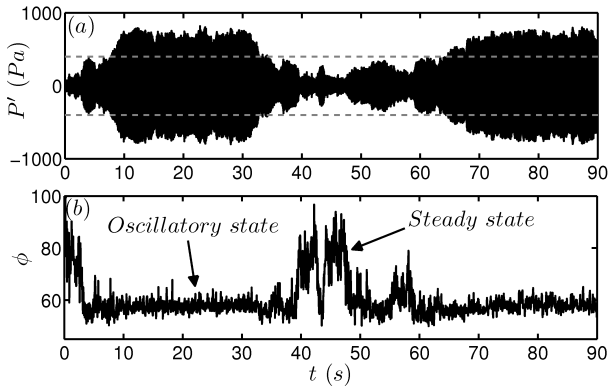

Figure 4.16: (a) Pressure evolution for noise level $57.2\ Pa$ at $X_f = 32.6$. (b) The evolution of ϕ of the system during the switching phenomenon.

The pressure traces acquired in the 40 experiments for six X_f values for a given noise level are used to construct the stability map of the system.

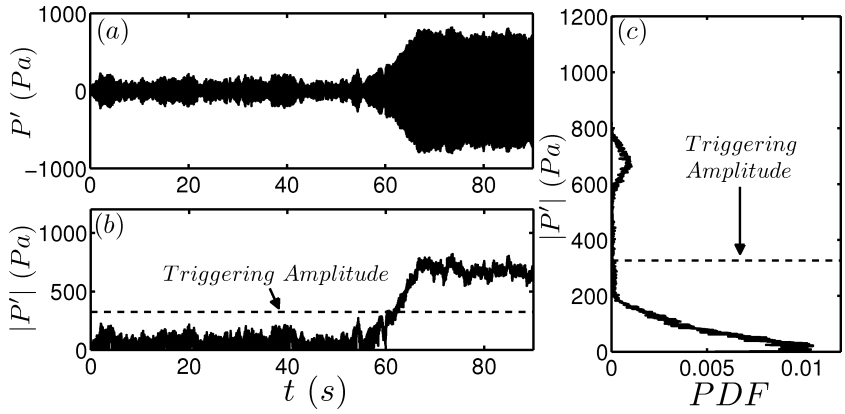

Figure 4.17: (a) The pressure trace of the system acquired from one of the experiments. (b) The extraction of the amplitude envelope. (c) Conversion of amplitude envelope data into stochastic stability curve.

The amplitude envelope of the pressure fluctuation are first extracted from the pressure trace acquired from the experiments (Fig. 4.17 a and b). Then the extracted amplitude envelope data is quantized into bins ranging from $0 - 1200\ Pa$ and with a bin size of $1\ Pa$. Once the amplitude data are quantized, the binned data are then normalized using the total number of the data points collected during the experiment, and then they are converted into PDF curves (Fig. 4.17 c). The PDF curves represent the probability of the system to stay in oscillatory state and steady state for a given X_f and noise level, in a time duration of $90\ s$. The area beneath the PDF curve between the triggering amplitude and limit-cycle amplitude gives the probability for the system to stay in

oscillatory state. The area beneath the PDF curve between steady state and triggering amplitude gives the probability for the system to stay in steady state. Since the system has different average transition time for different noise level and flame location, the predicted PDF will be different for different duration of operation, hence the predicted PDF curve are valid only for the $90\ s$ of operation. Using the PDF curves obtained for the six X_f the stochastic stability map is constructed. The stochastic stability maps are represented as a intensity map and they are overlaid on top of the deterministic bifurcation diagram to illustrate the system's preference to stay in steady state or limit-cycle orbit.

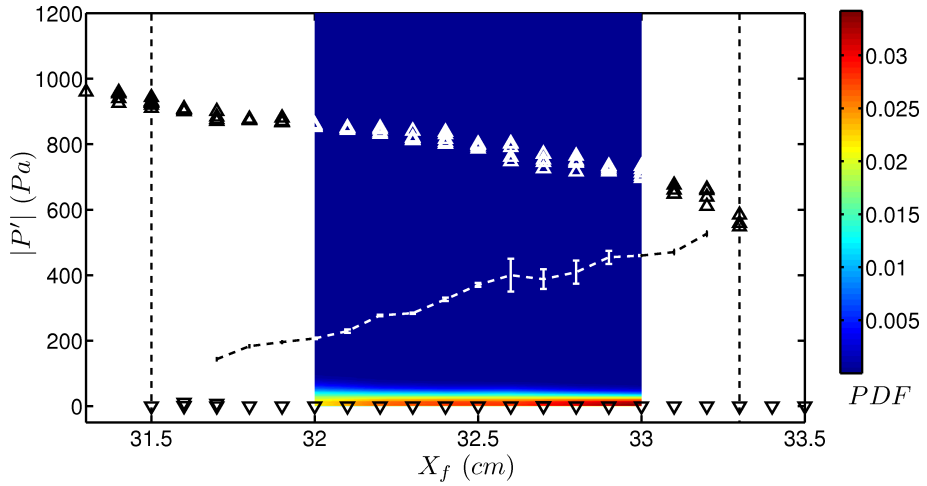

Figure 4.18: The stochastic stability map of the system for a noise level of $18.8\ Pa$.

The stability map for a noise level of $18.8\ Pa$ is shown in Fig. 4.18. The map shows that the system prefers to stay in steady state for the $90\ s$ operation of the system. The intensity distribution in the map is an outcome of the pressure trace that are shown in Fig. 4.13. The magnitude of noise level with which the system is perturbed, is represented by the standard deviation of the pressure fluctuations observed inside the combustion chamber and it is measured when the system is operating at $X_f = 33.5\ cm$ (see Section 4.2.2). But as the operating conditions are varied and approaches towards the deterministic Hopf point a unique feature is observed. We observe an increase in standard deviation (see Fig. 4.19), even when the forcing strength is maintained constant in the fuel plenum chamber. As the operating conditions approach the Hopf point the spurt formation becomes more prominent (Fig. 4.13) which causes the increase in standard deviation. Similar kind of observation was also observed in a numerical inves-

tigation of stochastically forced canonical shear flow performed by Farrell and Ioannou (1994). They observed a trend of increase in standard deviation as the Reynolds number (Control parameter) of the system was varied. They attributed this increase to the non-normal nature of the system. Hence the spurt formation observed in the system can also be attributed to the non-normal nature of the system.

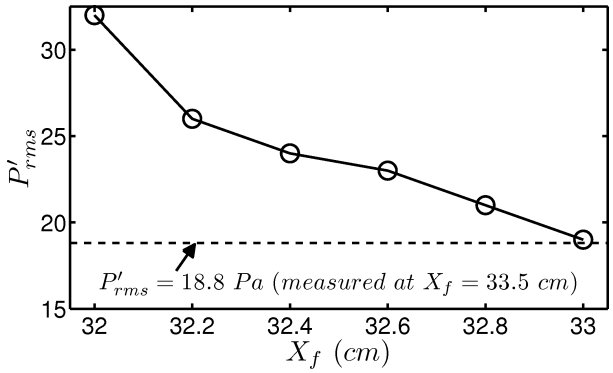

Figure 4.19: The variation of the standard deviation of the pressure trace as X_f is varied. The strength of forcing is kept constant at $25\ Pa$ inside the fuel plenum chamber.

The stochastic stability for a noise level of $38.8\ Pa$ is shown in Fig. 4.20. As the noise level in the system is increased, the system experiences NIT. At $X_f = 32\ cm$ the probability for transition increases to $98\ \%$ as the noise level is increased. Hence the threshold of stability has advanced from $X_f = 31.45\ cm$ to $X_f = 32\ cm$. From the stability map we can observe that the margin of linear stability shrinks (Lieuwen and Banaszuk, 2005). The reason for the system to have such high transition probability is due the nature of transition shown in Fig. 4.14 (g-i), where the system exceeds the threshold and directly reach the limit-cycle orbit directly.

As the noise level in the system is increased to $57.2\ Pa$, the threshold of linear stability is observed to advance further down to $X_f = 32.2\ cm$. This can be observed in the stochastic stability map of the system shown in Fig. 4.21. In the map we could observe formation of two finger like structures between the $X_f = 32.4\ cm$ and $X_f = 32.6\ cm$. These structures form due to the phenomenon of switching illustrated in Fig. 4.20 (d-f). Beyond $X_f = 32.6\ cm$ the system prefers to stay in steady state over the limit-cycle orbit.

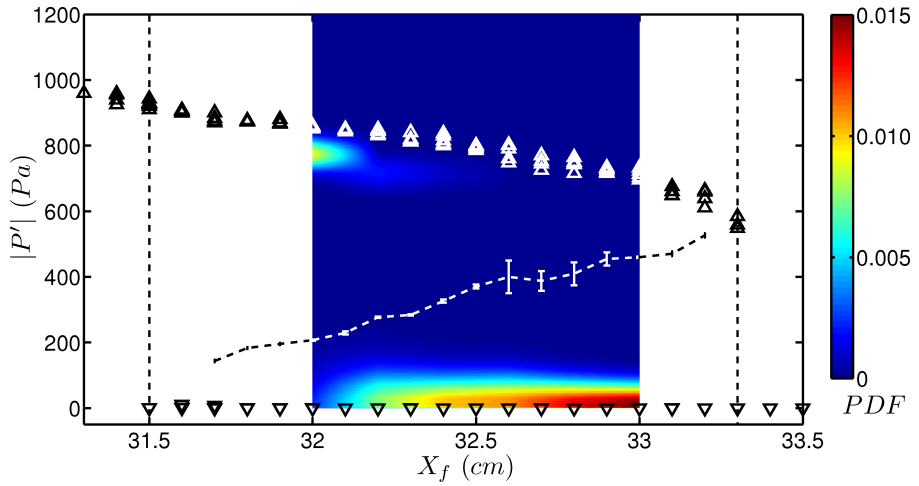

Figure 4.20: The stochastic stability map of the system for noise level of $38.8\ Pa$

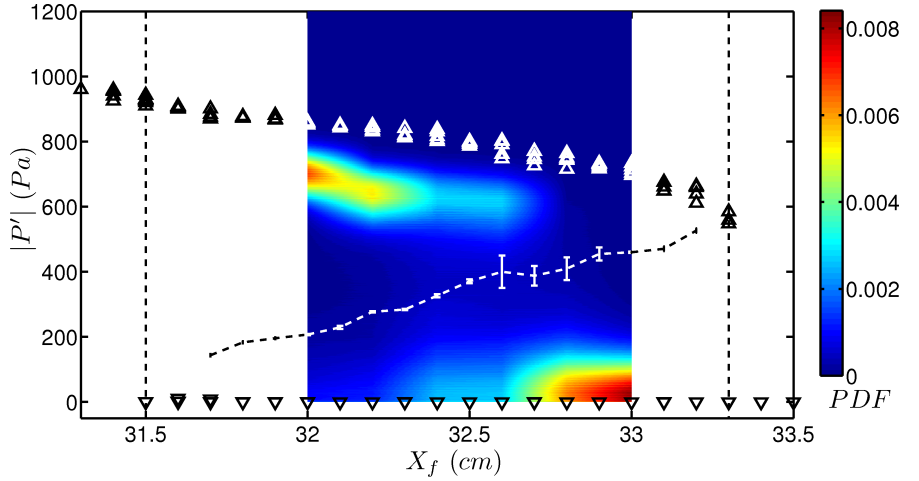

Figure 4.21: The stochastic stability map of the system for noise level of $57.2\ Pa$. Finger like structure observed between the $X_f = 32.4\ to\ 32.6\ cm$.

On further increasing the noise level to 100 Pa, the finger like structure further develop and bridge the steady state and oscillatory state of the system (see Fig. 4.22). The bridging structure is due to the nature of transition explained in Fig. 4.21 (g-h). For flame locations $X_f = 32.8\ cm$ and $X_f = 33\ cm$, we observed that the probability for system to experience NIT is above 50%. However, when the evolution of phase difference between P' and q' (ϕ) was investigated, we observe that the system did not experience any NIT and the system preferred to stay in steady state. The phase difference between P' and q' shows that system is out of phase throughout the evolution, but momentarily the amplitude of pressure fluctuation crosses well above the triggering amplitude, but the phase difference remains decoupled and the system quickly falls below the threshold (Fig. 4.23 a and b). From the switching phenomenon, we observed that the noise has the capability to stabilize the system. Thus on further increasing the noise level does not aid in triggering the system but it stabilizes the system. The noise level dislodges the system from oscillatory state and prefers to stay in stable state, hence the system is unable to sustain in the oscillatory state and reach the fold point. As a consequence, of this the system appears to undergo supercritical transition, though the system is undergoing subcritical transition (see Fig. 4.22). Further the amplitude of pressure fluctuation alone is not a good measure to identify whether a system is triggered; other parameters such as phase difference should also be considered.

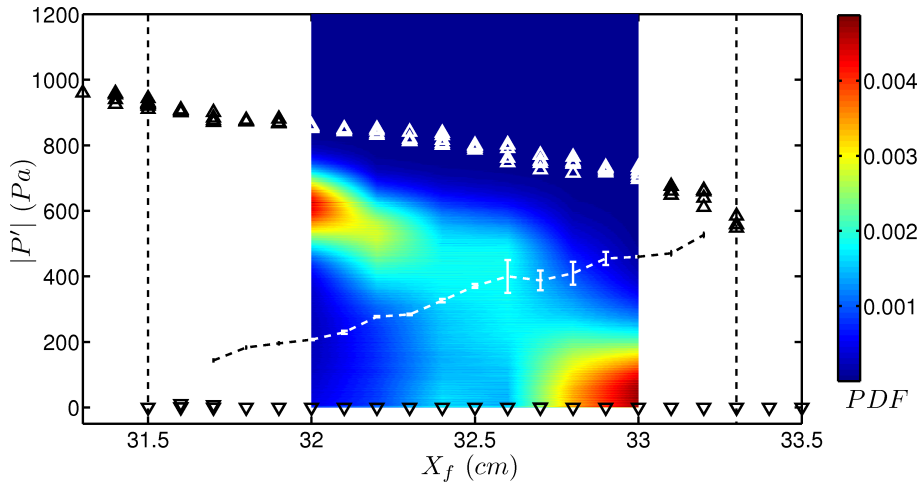

Figure 4.22: The stochastic stability map of the system for noise level of 100 Pa

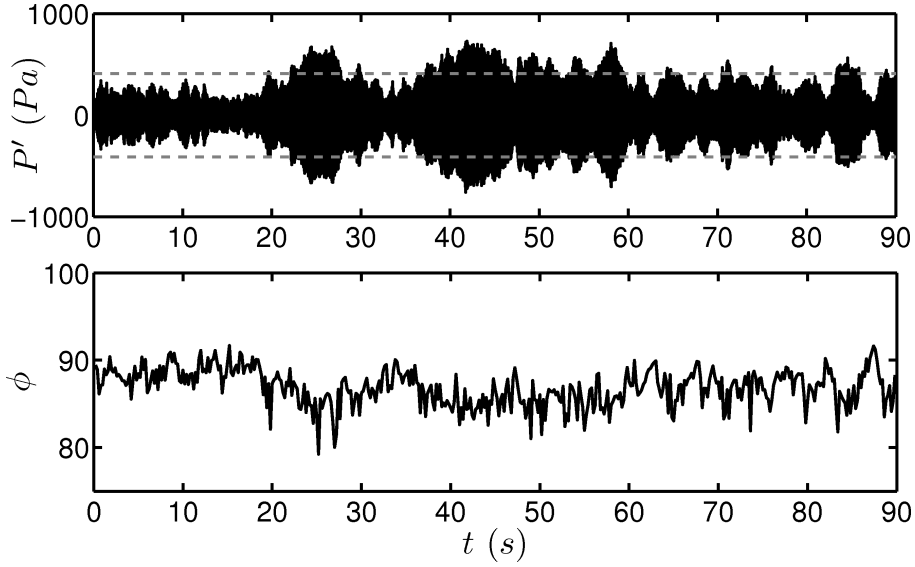

Figure 4.23: (a) Pressure evolution for noise level of $100\ Pa$ at $X_f = 32.8\ cm$. (b) The corresponding evolution of ϕ of the system.

4.2.8 Amplitude of oscillation

As the noise level in the system is increased, the amplitude of oscillation in the system is observed to decrease. The variation of amplitude with respect to the noise level is presented in the Fig. 4.24. In the absence of noise the system exhibits limit-cycle oscillations, which can be observed in phase portrait (Fig. 4.24). As the noise level in the system increases, the envelope of the trajectories in the phase portrait starts to shrink, representing a decrease in the amplitude of oscillations. This result is not in agreement with the finding from the theoretical study of Waugh and Juniper (2011), where the amplitude of the stable periodic solution in the presence of noise agrees well with that predicted by their noiseless simulations.

In the presence of noise the trajectory of the system does not close, and hence a band can be observed in the phase portrait. Under the influence of noise the phase difference between pressure fluctuation and heat release rate fluctuation drifts continuously (Lieuwen, 2001). This phase drift reduces the effective coupling between the pressure oscillations and fluctuating heat release rate and hence a reduction in amplitude of oscillation is observed. We define a quantity ζ which denotes the variation in Rayleigh integral in the presence of noise in comparison to a noise free case, where ζ is

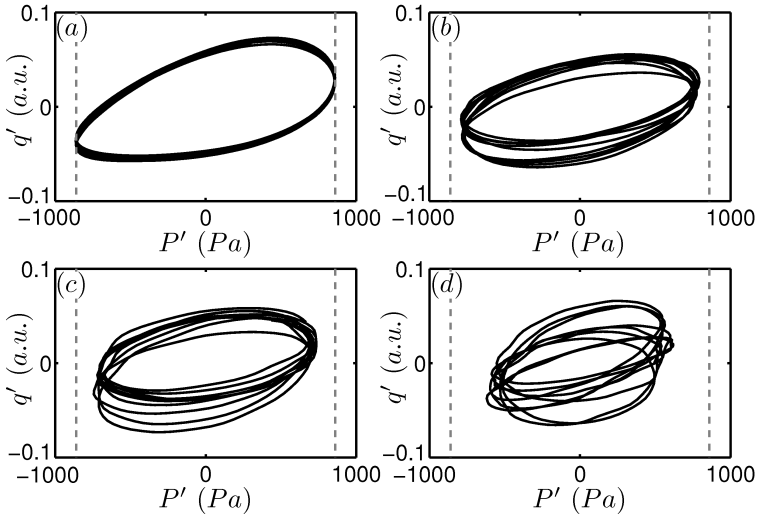

Figure 4.24: Phase portrait of the oscillatory state of the system at $X_f = 32\ cm$ for a noise level of (a) $0\ Pa$, (b) $38.8\ Pa$, (c) $57.2\ Pa$ and (d) $100\ Pa$. The dotted lines represents the limit cycle amplitude of the system for a noise free case.

defined as per the expression given in Eqn. 4.3

$$\zeta = \frac{\cos\phi - (\cos\phi)_{nonoise}}{(\cos\phi)_{nonoise}} \times 100 = \left[\frac{\int_0^T P'q'dt - \left(\int_0^T P'q'dt\right)_{nonoise}}{\left(\int_0^T P'q'dt\right)_{nonoise}} \right] \tag{4.3}$$

Table 4.3: The variation of coupling between P' and q' for various noise levels are presented. P'_{rms} represents the noise level in the system, $\bar{\phi}$ represents the average phase difference in the system and the $RMS(\phi)$ represents the standard deviation of the drifting ϕ, ζ represents the reduction in coupling between the P' and q'

$P'_{rms}\ (Pa)$	ϕ	$RMS(\phi)$	$\zeta\ \%$
0	58.6	0.3	0
38.8	60.2	0.8	4
57.2	62.8	1.3	8
100	64.5	2	14

The ζ represents the reduction in the coupling of P' and q' in the system as the noise level in the system is increased. The change in the coupling between P' and q' as the

noise level is varied in the system is presented in Table 4.3. Similar kind of observation was also observed by Berthet *et al.* (2003) in their experimental investigation of Faraday instabilities. They observed that in a noisy system the coupling between the forcing and fluid layer was disrupted. As a consequence the amplitude of oscillations were decreased. The presence of noise also acts as an additional damping in the system (Kabashima *et al.*, 1979).

CHAPTER 5

CONCLUSION AND OUTLOOK

In the present thesis, the effect of parametric noise on a thermoacoustic system is investigated experimentally. Experiments have been performed in a ducted non-premixed flame system. The investigation primarily focuses on the role of noise on the stability of a thermoacoustic system. The effect of noise on the thermoacoustic oscillation was also investigated. The salient conclusions of the investigation are as follows.

5.1 Conclusion

5.1.1 Deterministic state of the system

The stability of the thermoacoustic system in the absence of noise (deterministic system) was studied. The system is observed to undergo transition via subcritical Hopf bifurcation. As the system is excited at the triggering amplitude, the system evolves transiently towards an unstable periodic orbit, before growing to a stable periodic orbit, in a manner analogous to the bypass scenario proposed by Juniper (2011). During triggering the phase relationship between P' and q' was observed to evolve to overcome the threshold of triggering. The evolution of the system during triggering phenomenon was also observed in the phase portrait.

5.1.2 Noise induced transition

When the thermoacoustic system is perturbed with noise, it was observed to undergo transition from steady non-oscillatory state to oscillatory state. And it is termed as Noise Induced Triggering (NIT). The transition was observed in the system even when the amplitude of noise level is $1/8^{th}$ of the triggering amplitude of the deterministic system. Under the influence of noise, the system exhibits spurt formation which leads

to transient growth in the driving of the system and it aides the system to reach threshold of triggering. In the presence of small amount of noise, the system first grows towards an intermediate unstable attractor (the unstable periodic orbit) before eventually getting repelled to the final self-sustained oscillatory state, in agreement with the scenario proposed by Waugh and Juniper (2011). As explained by Fedotov *et al.* (2002), a stochastic dynamical system is fundamentally different from the corresponding deterministic system; the noise in effect, increases the degrees of freedom.

5.1.3 Reduction of stability margin

The threshold of stability of the system was observed to advance as the noise level in the system is increased. This reduces the stability margin of the system as predicted by Lieuwen and Banaszuk (2005). The occurrence of NIT causes the reduction of stability margin. furthermore, the transition has a probabilistic nature. The probabilistic nature is reflected in the stochastic stability map of the system as a smooth transition over a wide range of flame location, as proposed by Meunier and Verga (1988). The probability for the occurrence of NIT depends upon the noise level in the system. Also the probability increases as the operating parameters approach the Hopf point.

5.1.4 Switching phenomenon

For a particular noise level and flame location, the system was observed to switch between oscillatory state and noisy steady state. This shows that the noise is capable of disrupting the coupling and dislodge a system from a oscillatory state, and stabilize the system.

5.1.5 Bridging of two states

When the noise level is increased to higher value, it alters the nature of transition of the system. For a noise free case, the system undergoes transition via subcritical Hopf bifurcation. As noise level is increased the oscillatory state and non-oscillatory state of the system bridges together. At higher noise level the system is unable to sustain in

oscillatory state and reach the the fold point, thus the system appears to be undergoing transition via supercritical hopf bifurcation.

5.1.6 Reduction in amplitude of oscillation

During thermoacoustic oscillation, presence of noise disrupts the coupling between the P' and q'. This reduces the effective amplitude of oscillation. The noise acts as an additional damping in the system.

5.2 Future work

In the present investigation, the effect of parametric noise on the thermoacoustic system is investigated. The noise used in the experiments were of white in nature. As a next step one could investigate the effect of colored noise on the system. Waugh *et al.* (2011) has already performed numerical investigation for the above mentioned case and showed that different colored noise has different degree of impact on the system. In the present experiments it has shown that the noise is capable of stabilizing an oscillatory system. Thus one could further explore the aspect of noise induced stabilization by perturbing the system with different colored noise.

The formation of spurts was observed to play a vital role in triggering the system for low noise levels, but the mechanism that causes the spurt formation could not be investigated in detail. Investigations could be performed to understand the mechanism that causes spurt formation which will provide us an in depth knowledge on the role of noise in triggering the system.

APPENDIX A

CALCULATION OF REYNOLDS NUMBER

The Reynolds number of the flow in the brass tube and in the annular passage between brass tube and quartz tube is measured to ensure that the flow is stable so as to have low inherent fluctuation.

A mixture of Nitrogen and Methane in a volumetric ratio of $2:1$ is supplied through the central brass tube. The flow corresponds to a Hagen-Poiseuille flow. The Reynolds number for the flow can be calculated using the formula given in Eqn.A.1 (Mullin, 2011).

$$\mathrm{Re} = \frac{\rho_{mixture} v D}{\mu_{mixture}} \tag{A.1}$$

where

$\rho_{mixture}$ is density of Nitrogen-Methane mixture

v is average velocity of the mixture in brass tube

D is the diameter of the brass tube, $23.6 \times 10^{-3}\ m$

$\mu_{mixture}$ is the dynamic viscosity of the Nitrogen-Methane mixture.

The parameters like $\rho_{mixture}$ and $\mu_{mixture}$ for the Nitrogen-Methane mixture are computed using the formulas given in Eqn. A.2 and A.3 (NAG, 2005).

$$\rho_{mixture} = \frac{\rho_1 V_1 + \rho_2 V_2 + \rho_3 V_3 ..... \rho_n V_n}{V_1 + V_2 + V_3 ..... V_n} \tag{A.2}$$

where

ρ_n is the density of the constituent gases

V_n is the volume of the constituent gases

So for the Nitrogen-Methane mixture $\rho_{N_2} = 1.185\ kg/m^3$, $V_{N_2} = 2\ litre$, $\rho_{CH_4} =$

$0.68\ kg/m^3$, $V_{CH_4} = 1\ litre$

$$\rho_{N_2+CH_4} = \frac{(1.185 \times 2) + (0.68 \times 1)}{2+1} = 1.016 kg/m^3$$

$$\mu_{mixture} = \frac{\sum \chi_n \mu_n \sqrt{M_n}}{\sum \chi_n \sqrt{M_n}} \tag{A.3}$$

where

μ_n is the dynamic viscosity of the constituent gases

M_n is the molecular weight of the constituent gases

χ_n is the mole fraction of the constituent gases in the mixture, and

$$\chi_n = \frac{\left(\frac{\rho_n V_n}{M_n}\right)}{\sum_1^n \left(\frac{\rho_n V_n}{M_n}\right)}$$

for Nitrogen-Methane mixture $\mu_{N_2} = 0.0000165\ Pas$, $M_{N_2} = 28.0134\ kg/kmol$, $\mu_{CH_4} = 0.0000102\ Pas$, $M_{CH_4} = 16.0430\ kg/kmol$, $\chi_{N_2} = 0.66$, $\chi_{CH_4} = 0.34$

$$\mu_{N_2+CH_4} = \frac{\left(0.6666 \times 0.0000165 \times \sqrt{28.0134}\right) + \left(0.3334 \times 0.0000102 \times \sqrt{16.043}\right)}{\left(0.6666 \times \sqrt{28.0134}\right) + (0.3334 \times 0.0000102)}$$

$$\mu_{N_2+CH_4} = 0.0000147 Pas$$

and the Reynolds number is

$$\mathrm{Re} = \frac{1.016 \times 0.121 \times 23.6 \times 10^{-3}}{0.0000147} = 197.36$$

The critical Reynolds number for a flow through pipe is $\mathrm{Re}_{critical} = 2300$ (Mullin, 2011)

The Reynolds number of the flow in the annular passage can be calculated using the

formula given in Eqn.A.4

$$\mathrm{Re}_{annular} = \frac{\rho_{Oxygen} v D}{\mu_{Oxygen}} \tag{A.4}$$

Where

ρ is density of Oxygen

v is average velocity of the gas in the annular space

D is the hydraulic diameter of the annular space and it is defined as $D = d_{outer} - d_{inner}$, d_{outer} and d_{inner} are the outer and inner diameter of the annular space respectively

μ is the dynamic viscosity of the Oxygen

for Oxygen $\rho_{oxygen} = 1.354\ kg/m^3$ and $\mu_{oxygen} = 0.000019 Pas$

$$\mathrm{Re}_{annular} = \frac{1.354 \times 0.026 \times (0.047 - 0.025)}{0.000019} = 40.76$$

The critical Reynolds number for a flow in a annular passage is $\mathrm{Re}_{critical} = 1600$ (Sheen *et al.* (1997)). Thus the flow in both brass tube and annular passage are ensured to be laminar.

APPENDIX B

CALIBRATION OF PRESSURE TRANSDUCER ADAPTERS

The pressure transducers are flush mounted on the setup using a teflon adapter. The dimensions of the adapter are presented in Fig.B.1. To ensure that the teflon adapter does not affect the pressure measurement a calibration test was performed. Towards this purpose, one transducer PCB $1030B02\ SN-5520$ is chosen as reference transducer, it has a sensitivity of $219.46\ mV/kPa$. The schematic of the calibration setup is shown in Fig. B.2. The calibration setup has an acoustic resonator of length $1\ m$ and and it has a diameter (d_{reso}) of $50\ mm$. The resonator has a cut-off frequency of $f_{cut} = 8000\ Hz$, for the propagation of radial modes in the duct (referred from Kinsler *et al.* (2000))). The frequency of interest for our present investigation is ranges from $50-2000\ Hz$, which is much less than the f_{cut} frequency. Thus only longitudinal modes propagate in the duct. An 'AHUJA AH-60' acoustic driver unit is mounted at one end of the tube and on the other side an end plate is provided to mount the transducer for calibration (Fig. B.3).

The calibration is preformed as follows. The calibration set up was excited at a specific frequency for $3\ s$. The amplitude of pressure oscillation inside the duct is at the end plate is measured simultaneously by the reference transducer and the transducer to be calibrated. From the collected pressure trace the amplitude ratio and phase between the reference transducer and the transducer to be calibrated is calculated. The resolution of the frequency is $1\ Hz$. The frequency response of the teflon adapter with the $1030B02\ SN-5519$ transducer is acquired and the data is presented in Fig. B.4. The variation of amplitude ratio for various frequency is less than 5% and the corresponding calibration constant is 0.997. The phase difference in the measured pressure trance is also negligible and hence it can also be neglected. The schematic representation of the setup is presented in the Fig. B.5

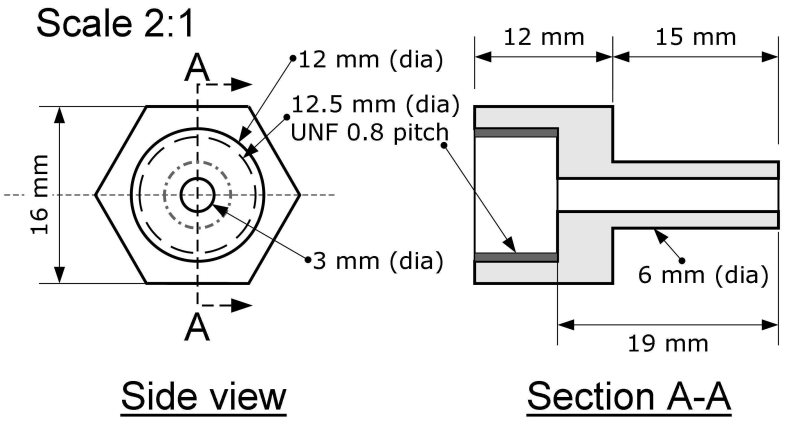

Figure B.1: Dimensions of the teflon adapter used to mount the transducer

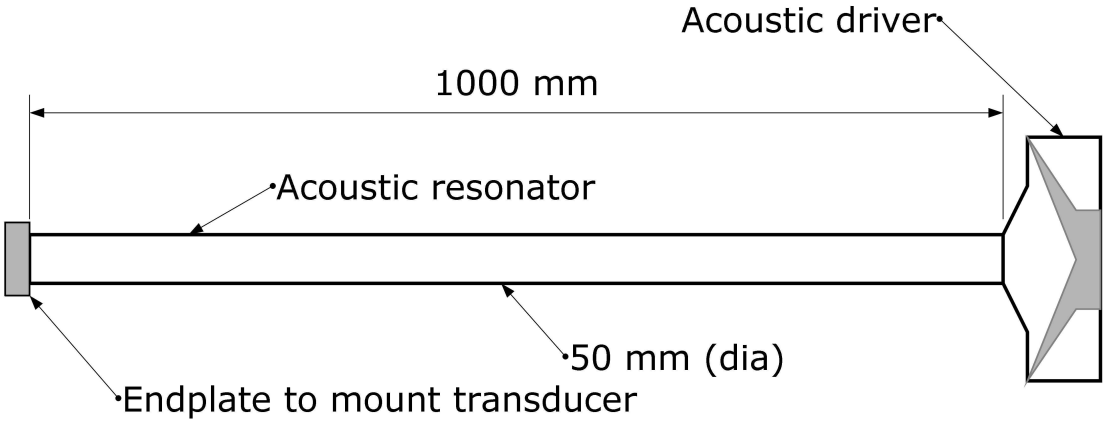

Figure B.2: Schematic view and dimensions of the calibration set up

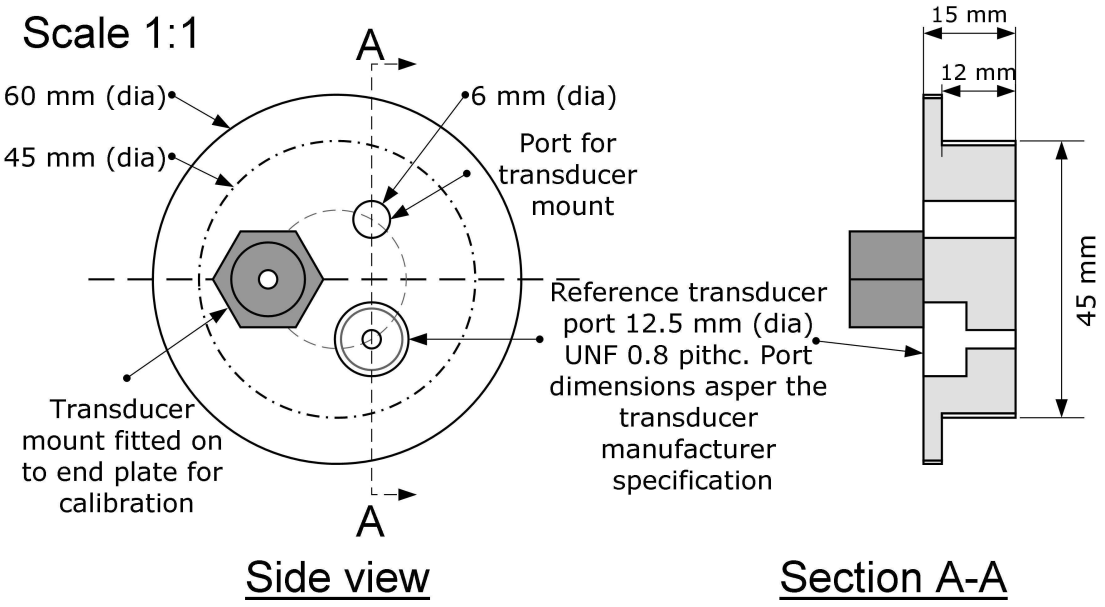

Figure B.3: Dimensions of the endplate used in the calibration setup

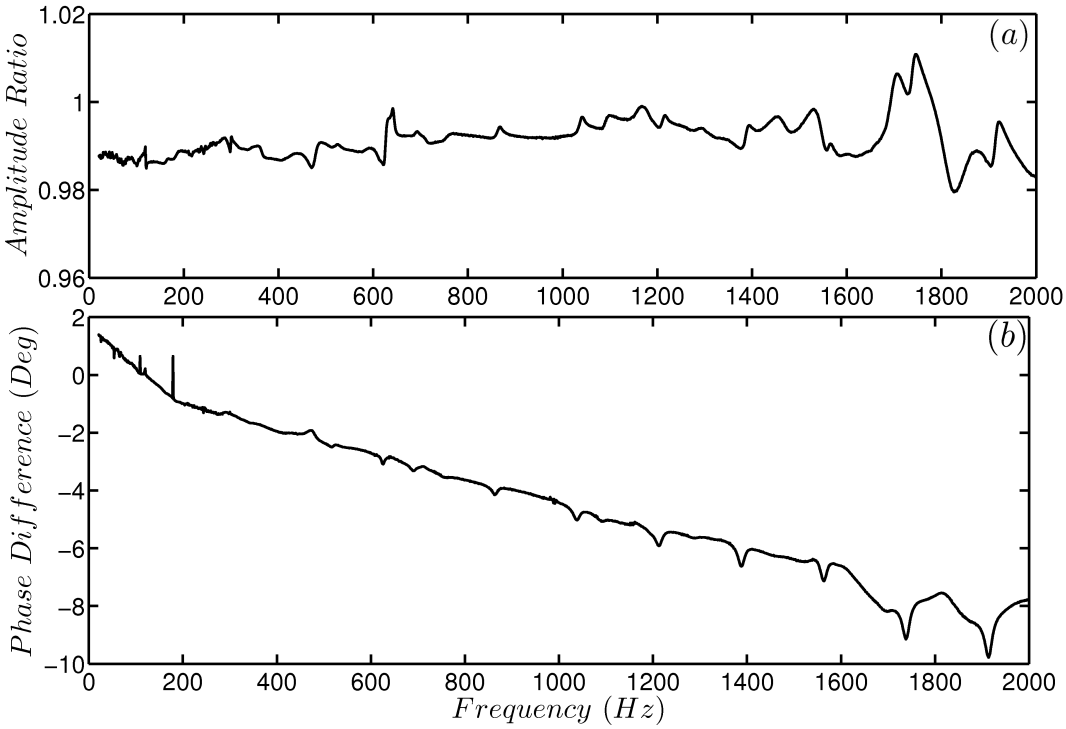

Figure B.4: The frequency response (a) and phase difference (b) of the teflon adapter for a frequency range of $20 - 2000\ Hz$.

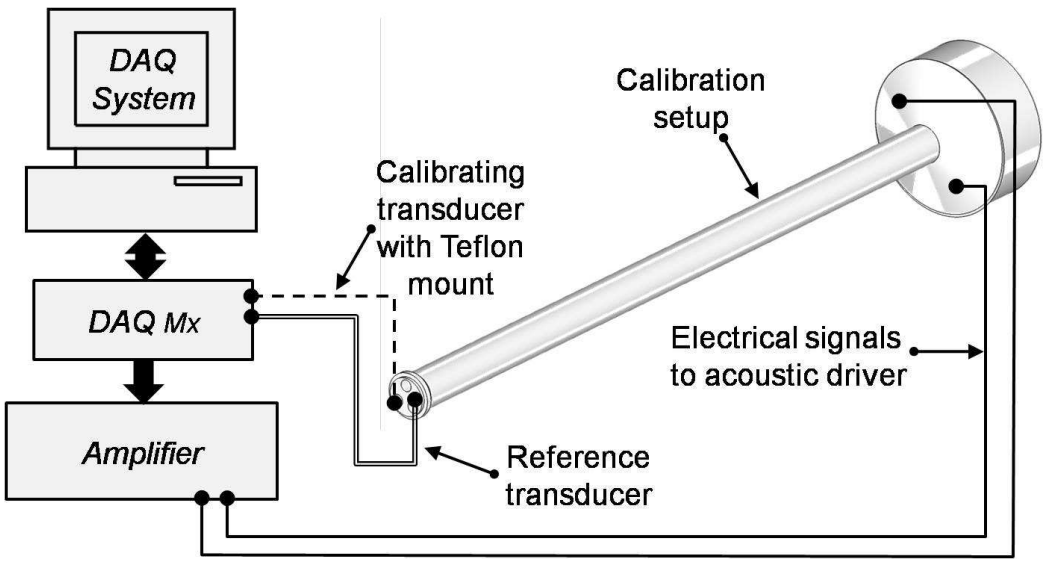

Figure B.5: Schematic representation of the calibration setup

APPENDIX C

VALIDATION OF OH^* MEASUREMENT AS A REPRESENTATIVE OF HEAT RELEASE RATE

In an effort to measure the instantaneous heat release rate from the flame a suitable method has to be identified. Normally CH^* chemiluminescence is measured to measure the instantaneous heat release rate of the system, but they are valid only for premixed flame and for a particular equivalence ratio only. Hence a suitable indicator has to be chosen to measure the instantaneous heat release rate. The emission spectrum of the flame for $\phi = 1$ was acquired using a 'Aventes spectrum analyzer'. The emission spectrum of the flame is shown in Fig. C.1(a). We can observe that there is a black body radiation from soot and emission corresponding to OH^* chemiluminescence. To validate that the OH^* emission can be utilized to measure the instantaneous heat release rate, a validation test was performed.

The validation was performed as follows. The collection fibre was located at a distance of $25\ cm$ from the flame (see Fig. C.2). The flow rate of fuel was varied in steps of $100\ ccm$ by maintaining $\phi = 1$ as constant and the emission spectrum data of the flame was acquired. From the collected emission spectrum the area beneath the emission spectrum curve between $300\ to\ 315\ nm$ was measured, this represents the strength or intensity of the OH^* emission. The data of the variation of the OH^* emission for fuel flow rate is shown in Fig. C.1 (b). The fuel flow rate indirectly represents the heat release rate of the system. We can observe that there exist a linear relationship between the strength of the OH^* emission and the heat release rate of the flame. Hence we could use the OH^* as an indicator of the heat release rate of the system.

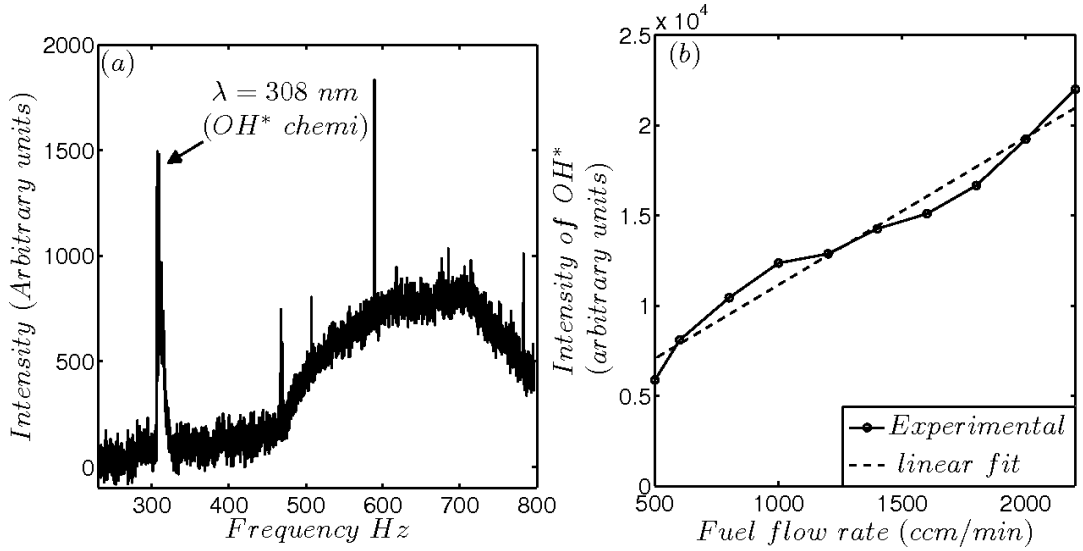

Figure C.1: (a) Emission spectrum of the flame showing peak at $308\ nm$ wavelength. (b) Variation of intensity of OH^* signal as the mass flow rate of the fuel is increased maintaining $\phi = 1$ as constant

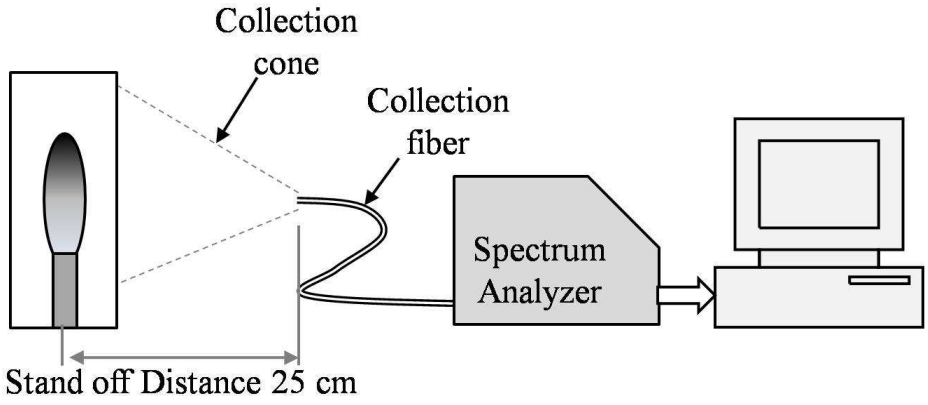

Figure C.2: Validation experiment for chemiluminescence

APPENDIX D

CHARACTERIZATION OF SPEAKER

In order to perturb the system, we have installed a 6" sub woofer directly to a fuel plenum chamber. To quantify the ability of the speaker to recreate the signal we perform a characterization test on the speaker. First the test is to quantify the ability of the speaker to recreate the sinusoidal signal is assessed by measuring the 'Total Harmonic Distortion (THD)' for frequencies ranging from $20 - 1000\ Hz$. THD is defined as the ratio of the sum of the powers of all harmonic components to the power of the fundamental frequency. And it is given by the expression in Eqn. D.1.

$$\%ofTHD = \frac{P_2 + P_3 + P_4 + ... + P_\infty}{P_1} \times 100 = \frac{\sum_{n=2}^{\infty} P_n}{P_1} \times 100 \qquad \text{(D.1)}$$

Where

P_1 is the power present in the fundamental frequency of the produced acoustic signal.

P_n is the power present in the harmonics of the produced acoustic signal.

The speaker is excited by a sinusoidal signal of known frequency, then the acoustic signal generated by the speaker is then acquired using pressure transducers. The collected data is then processed and the '$\%\ of\ THD$ of the signal is computed. The THD of the speaker for various frequencies are presented in Fig. D.1. For frequencies below $20\ Hz$ the THD is as high as 13%. Above $20\ Hz$ the THD levels are well below 5%. This ensures that the speaker will always perturb the system in the desired frequency during excitation for a frequency range $20 - 1000\ Hz$.

To quantify the ability of the speaker in generation of noise a different test is performed. A Gaussian white noise is generated for a frequency bandwidth of $0-5000\ HZ$ and was supplied to the speaker. The noise generated by the speaker is then acquired through transducer and it was processed to get the frequency spectrum. The frequency

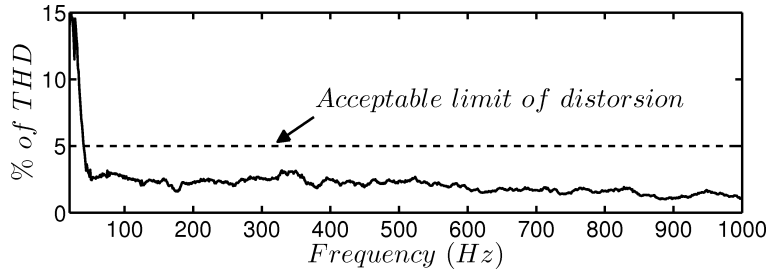

Figure D.1: THD of the speaker for the frequency range of $1 - 1000\ Hz$.

spectrum is presented in Fig. D.2, we can observe that the spectrum is considerably linear between the $20 - 2000\ Hz$. When the slope of the spectrum line between $20 - 2000\ Hz$ is investigated it has a slope of $0.02\ dB/octave$, which can still be considered as white noise. Since the flame acts as a low pass filter and the response of the flame to high frequencies is weak (Klein, 2000) the flame effectively sees a white noise. The cut-off frequencies ($20\ \&\ 2000\ Hz$) associated with the noise is very larger than all relevant frequencies of the system and it has flat spectrum, such noise is defined as 'quasi-white noise' (Horsethemke and Lefever, 1984; Kabashima *et al.*, 1979). When the distribution of the amplitude of the pressure fluctuation is observed (Fig. D.2 b), the distribution is of Gaussian in nature. Hence from the noise produced by the speaker is a 'Gaussian quasi-white noise' between the frequency range of $20 - 2000\ Hz$, where the higher cutoff frequency is 10 times greater than the eigen-frequency of the system.

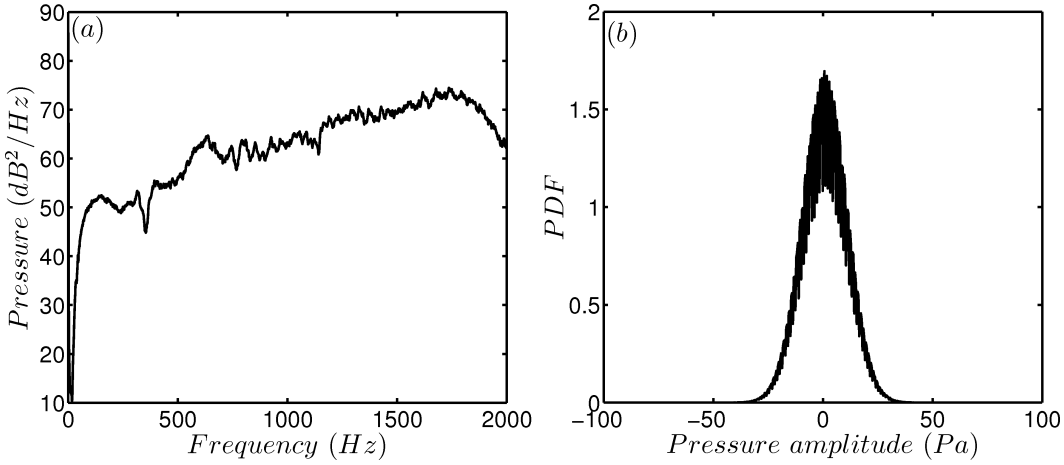

Figure D.2: (a)Power spectral density of the white noise generated by the speaker. (b)PDF of the amplitude distribution of the noise.

APPENDIX E

VELOCITY FLUCTUATION MEASUREMENTS AT THE TIP OF THE BURNER

We are perturbing fuel flow rate of the system randomly in an effort to understand NIT. To perturb the fuel flow rate of the system we have installed a speaker in the fuel plenum chamber. When an electrical signal is provided to the speaker the diaphragm fluctuates and varies the volume of the fuel plenum chamber, thus oscillating the fuel flow rate of the system. We are interested in identifying the magnitude of the velocity fluctuation at the tip of the burner and the profile of the random fluctuation at the tip of the burner with out flame (cold flow condition). To quantify the fluctuation at the tip of the burner velocity measurements were performed.

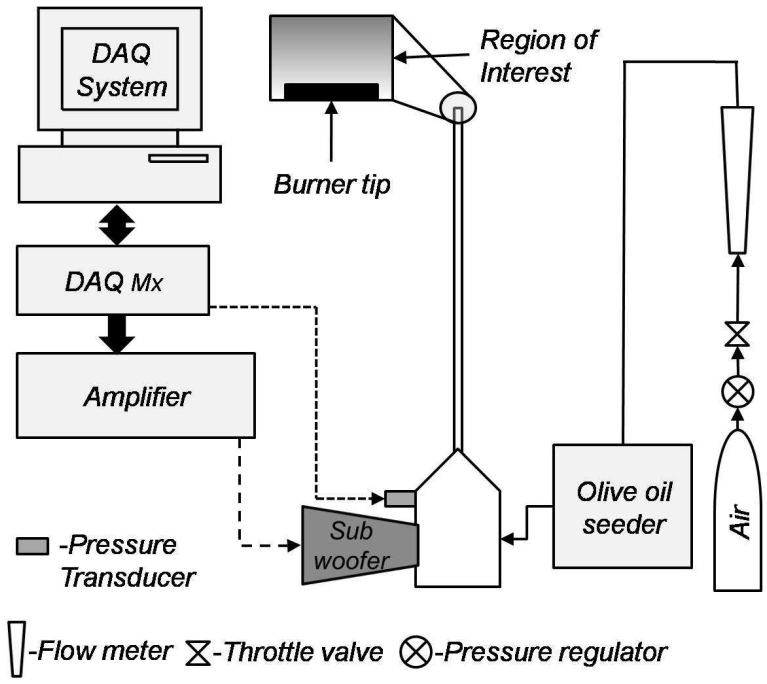

Figure E.1: Schematic representation of the set up considered for velocity measurements

The velocity at the tip of the burner was measured using two techniques. The unperturbed flow was measured using Laser Doppler Velocimetry (LDV). The data col-

lected through LDV measurements were used as a benchmark to quantify the velocity measured through High Speed Particle Image Velocimetry (HS-PIV). Through this comparison the parameters of the HS-PIV were optimized to capture the random fluctuations. The measurements through LDV and HS-PIV were performed independently. A schematic of the part of the setup considered for investigation is shown in Fig. E.1.

In order to perform the measurements in cold flow condition the fuel (mixture of Methane and Nitrogen) is replaced by air as a flow medium. The properties of air and fuel is presented in the Table E.1. From the data provided in the Table E.1 we can observe that the flow properties of both the medium are almost same, thus the dynamic behaviour of both the gases will be same, the measurements obtained for air can be compared to the fuel. The properties of the air were acquired from the Scientifique (1976).

Table E.1: Comparison of properties of air and fuel.

$Properties$	$Fuel$	Air
Density	$1.016\ kg/m^3$	$1.102\ kg/m^3$
Dynamic viscosity	$0.0000147\ Pas$	$0.0000169\ Pas$
Reynolds number	197.3	197.9
Entry length	$0.22\ m$	$0.23\ m$

E.1 Laser Doppler Velocimetry

A TSI Laser Doppler velocimetry system was used to measure the velocity at the exit of the burner tube. A single component measurement parallel to the axis of the Burner tube was acquired. LDV measurements were acquired to characterize the unperturbed flow field of the experimental setup. The interrogation volume diameter is $163\ \mu m$ and the focal length of the probe was $363\ mm$. The average rate at which the data was collected is $990\ samples\ per\ second$. The focal length of the probe used was . The collected data is processed using TSI Flowsizer software.

The velocity at the center of the burner tube was measured. The velocity trace acquired from the system is shown in the Fig. E.2 (a). The measurement was conducted

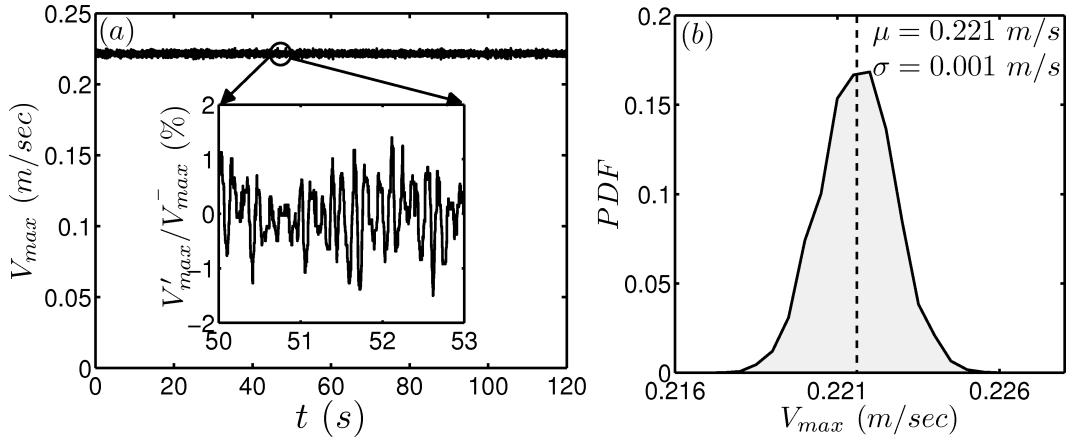

Figure E.2: (a) evolution of V_{max} in the center of burner tube. (b) PDF of the velocity data. The system has inherent fluctuation of less than 1% of the mean value.

until 1×10^5 samples were collected. It was observed from the velocity trace that the flow has an inherent fluctuation. The probability density function was computed for the Velocity trace and is shown in the Fig. E.2 (a) and the mean of the velocity trace was observed as $V^{-}_{max} = 0.221\ m/s$ and the standard deviation $\sigma = 0.001\ m/s$. The velocity trace was normalized with V^{-}_{max} and the fluctuating velocity (V'_{max}) over the mean value is shown in the inset in Fig. E.2 (a). From the normalized velocity trace and σ it can be clearly observed that the fluctuation of velocity is less than 1%. This ensures that the flow is laminar (Darbyshire and Mullin (1995)).

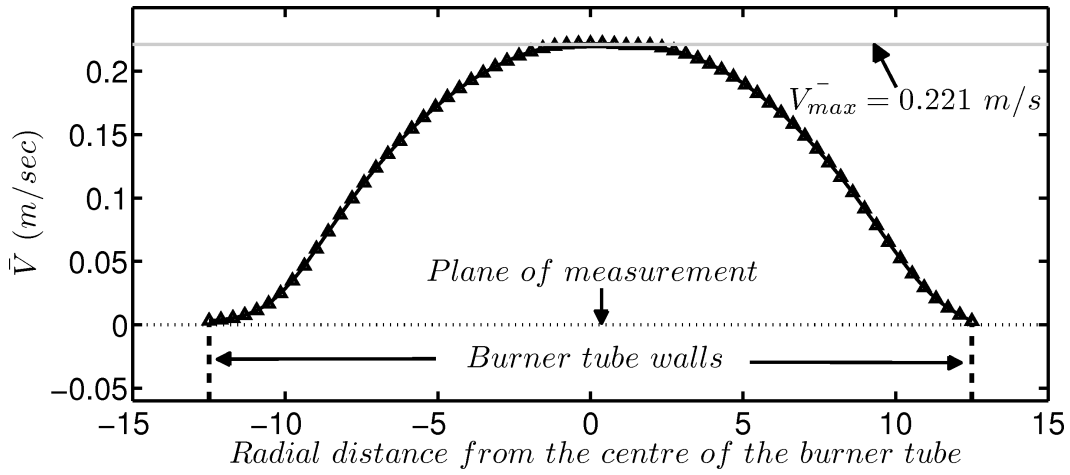

Figure E.3: The velocity profile at the exit of the burner tube for the fuel flow rate mentioned in Table 3.2. The dashed lines represents the location of the walls of the burner. The dotted lines represent the plane of measurement which is $2\ mm$ from the tip of the burner.

The LDV measurements were made across the diameter of the burner tube and the velocity profile of the jet at the exit of the burner tube was obtained and the velocity profile is shown in Fig. E.3. The velocity profile at the exit of the burner tube was observed to be parabolic in nature, similar to a profile of a fully developed Hagen-Poiseuille flow (Rankin *et al.*, 1983; O'Neill *et al.*, 2004). The average velocity of the gases flowing through the burner tube was calculated using the formula given in Eqn. E.1 (White, 2010).

$$V_{avg} = \frac{1}{R^2} \int_{-R}^{R} u(r) r dr \tag{E.1}$$

where

V_{avg} is the average velocity of the gases flowing through the burner tube.

R is the radius of the burner tube and it's magnitude is $11.8\ mm$

$u(r)$ is the velocity of the gases at the location r from the center of the tube.

The average velocity was calculated from the velocity profile obtained through LDV measurement and the magnitude is $\bar{V_{avg}} = 0.122\ m/s$.

E.2 High Speed Particle Image Velocimetry

To capture the evolution of the velocity fluctuations at the exit of the burner high speed PIV technique was implemented (Raffel *et al.*, 1998). Since the flow was perturbed with a white noise of frequency bandwidth $20 - 2000\ Hz$ a sampling rate of $8000\ frames\ per\ second\ (FPS)$ was chosen ($\Delta t = 125\ s$). The chosen sampling rate is twice the sampling frequency recommended by Nyquist-Shannon theorem. An over sampling is utilized here to capture the random velocity fluctuations with higher temporal resolution.

To capture the image of the oil particles at such high frame rate, a Phantom $V12.1$ high speed imaging system was used. Phantom $V12.1$ camera is a CMOS camera with 1200×800 pixel detector. The camera is controlled by phantom camera control software (version 1.0). The camera was operated with a maximum exposure of $120\ \mu s$. To

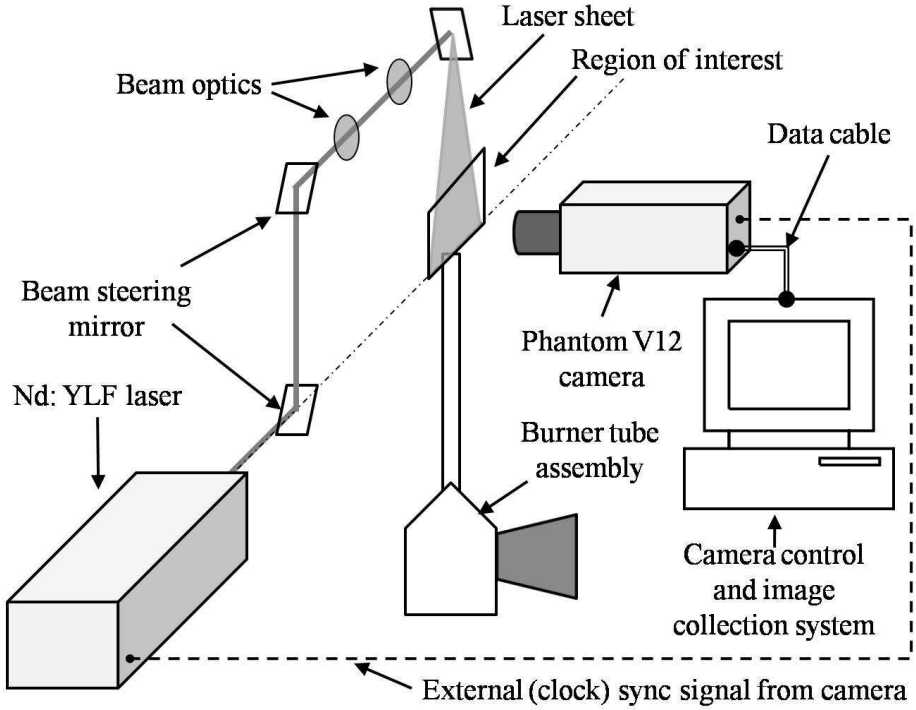

Figure E.4: The velocity profile at the exit of the burner tube for the fuel flow rate mentioned in Table 3.2. The dashed lines represents the location of the walls of the burner. The dotted lines represent the plane of measurement which is $2\ mm$ from the tip of the burner.

illuminate the particles at 8000 Hz a Photonic Industries Nd:YLF laser lasing at 532 nm was used. The laser when operated at $8000\ Hz$ it delivers a laser pulse of $10.01\ mJ$ of energy. The width of the laser pulse is $50\ ns$. A combination of lenses and mirrors were used to steer and focus the beam into the region of interest. The path of the beam is shown in the Fig. E.4. The laser and the camera are synchronized together using the synch pulse generated in the camera. When the camera opens its shutter an on board signal generator produces a $5\ V$ Transistor-transistor logic (TTL) pulse with 50% duty cycle. The signal is acquired through from the camera through an $F - sync$ port and the signal is supplied to laser in the external sync port. The lasers internal frequency generator is turned off and made to operate in external clock mode. Whenever the camera opens its shutter the laser flashes after some time delay. This time delay is a unknown parameter, but it is a constant for a given system. The timing diagram for the laser and camera synchronization is given in the Fig. E.5.

The high speed imaging system records a high speed video footage of the flow field. Later images are extracted from the video file and saved as a single exposure images.

The velocity of the flow field is computed by using $PIVview\ 2C\ software$. The single exposed images are loaded and the velocity field are computed for the subsequent images, for example the velocity field is computed by cross correlating the image n and the image $n+1$ and generates a velocity data file, then next flow field is computed by cross correlating images $n+1$ and $n+2$. So for N images we get N-1 velocity data. The output velocity data of the $PIVview\ 2C$ software is read in $MATLAB$ and further post processing are performed to build the time evolution of the flow field.

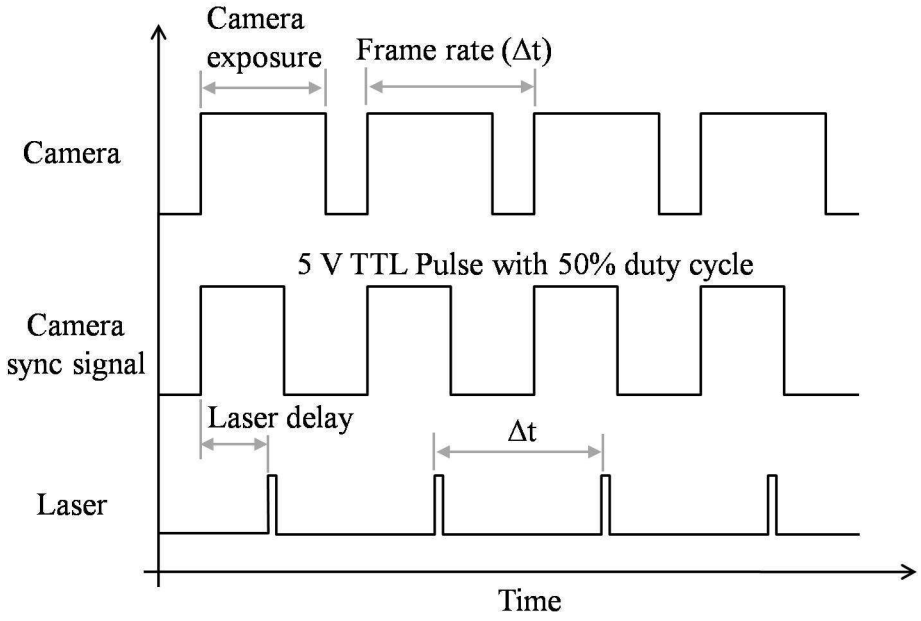

Figure E.5: Timing diagram for the high speed PIV system

E.2.1 Velocity profile

The velocity profile at the exit of the burner tube is measured using the HS-PIV technique. A 8001 images were acquired and 8000 velocity field data was obtained, then an ensembled average flow field data was obtained. The acquired velocity profile was compared with the velocity profile acquired through LDV.

The comparison between velocity profile acquired through HS-PIV and LDV are shown in Fig. E.6. The results from HS-PIV are in close agreement with the results of LDV. The quantities of the velocity profile acquired from the HS-PIV data was also found to be in good agreement with the LDV data (Table E.2). Thus the parameters of

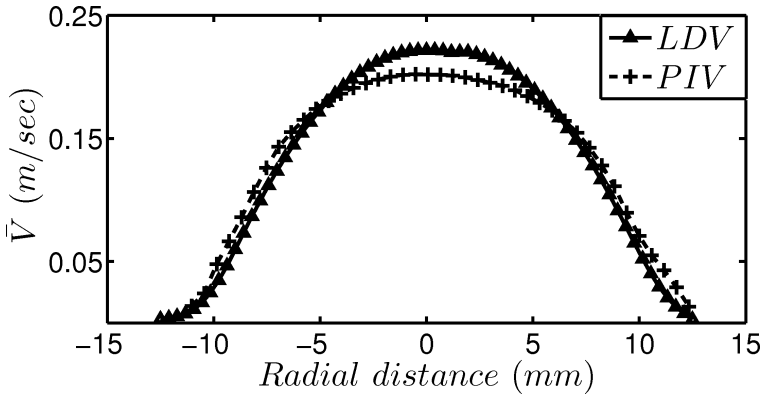

Figure E.6: Timing diagram for the high speed PIV system

HS-PIV have been optimized to measure the evolution of flow field. The fuel flow rate of the system is approximately equal to V_{avg}, in order to define the fuel volume flow rate fluctuation the evolution of V_{avg} at the tip of the burner is monitored.

Table E.2: Comparison of data obtained from HS-PIV and LDV.

$Quantity$	LDV	$HS-PIV$	$Error$
$\bar{V_{avg}}$	$0.122\ m/s$	$0.127\ m/s$	4.8%
$\bar{V_{max}}$	$0.221\ m/s$	$0.211\ m/s$	4.3%

E.2.2 Randomly perturbed flow field

The random perturbations are imparted to the flow by adding Gaussian quasi-white noise to the system through the speaker. The strength of the noise with which the flow field is perturbed is represented by P'_{rms} observed inside the fuel plenum chamber. After imparting Gaussian quasi-white noise, the corresponding fluctuation in V_{avg} is observed. The trace of the pressure fluctuation observed inside the plenum chamber and the corresponding V_{avg} observed at the tip of the burner is presented in Fig. E.7. The V_{avg} fluctuation at the tip of the burner is quantified by the $RMS\ of\ V_{avg}$. The FFT of the velocity fluctuation is shown in Fig. E.8 (a). The spectrum was observed to have peaks at discrete frequencies. The peaks corresponds to the natural frequency of the burner tube assembly. When noise is added to the system, the acoustic field amplifies the frequencies corresponding to the natural frequencies of the burner assembly. The

statistical quantities of the pressure fluctuation and the velocity fluctuations were computed and the profile of the amplitude distribution was investigated (Fig. E.8 b). The Pressure and velocity was observed to have a Gaussian profile.

The magnitude of the noise imparted to the system is varied and the corresponding velocity fluctuation at the tip of the burner is acquired. From the acquired data a transfer function was constructed between various noise levels P'_{rms} and the corresponding $RMS\ of\ V_{avg}$ observed at the tip of the burner (Fig. E.9).

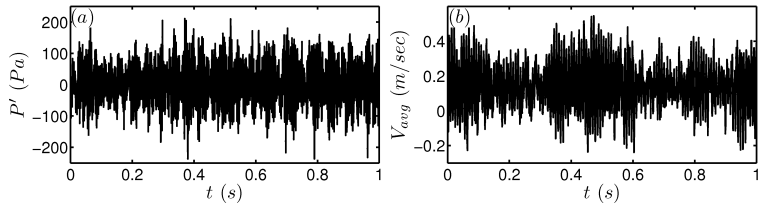

Figure E.7: (a) pressure trace observed in the fuel plenum chamber. (b) The V_{avg} observed at the tip of the burner.

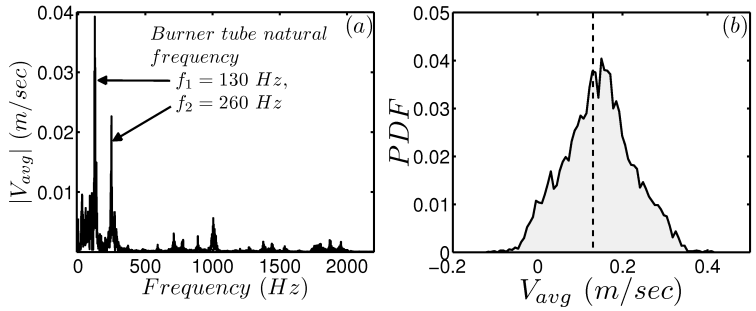

Figure E.8: (a) Spectrum of V'_{avg} at the tip of the burner tube when perturbed with noise. (b) Distribution of the amplitude of velocity fluctuation.

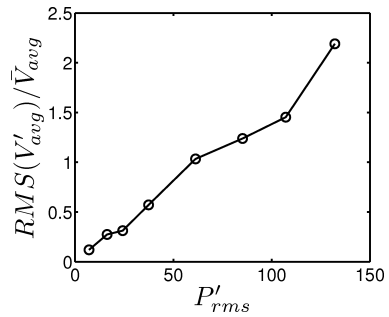

Figure E.9: transfer function constructed between P'_{rms} and $RMS(V'_{avg})$

REFERENCES

1. **Arnold, L.**, *Random dynamical systems*. Springer monographs in mathematics. Springer, 1998. ISBN 9783540637585.

2. **Balakrishnan, V.**, *Elements of nonequilibrium statistical mechanics*. Ane Books, 2008. ISBN 9781420074192.

3. **Balasubramanian, K.** and **R. I. Sujith** (2008*a*). Non-normality and nonlinearity in combustion acoustic interaction in diffusion flames. *Journal of Fluid Mechanics*, **594**, 29–57.

4. **Balasubramanian, K.** and **R. I. Sujith** (2008*b*). Thermoacoustic instability in a Rijke tube: Non-normality and nonlinearity. *Phys. Fluids*, **20**, 044103.

5. **Bendat, J. S.** and **A. G. Piersol**, *Random Data: Analysis and measurement procedures*. John Wiley and sons, New York, 1986, second edition.

6. **Berthet, R.**, **A. Petrossian**, **S. Residori**, **B. Roman**, and **S. Fauve** (2003). Effect of multiplicative noise on parametric instabilities. *Physica D: Nonlinear Phenomena*, **174**, 84 – 99. ISSN 0167-2789. URL `http://www.sciencedirect.com/science/article/pii/S016727890200684X`.

7. **Billings, L.**, **I. B. Schwartz**, **D. S. Morgan**, **E. M. Bollt**, **R. Meucci**, and **E. Allaria** (2004). Stochastic bifurcation in a driven laser system: Experiment and theory. *Phys. Rev. E*, **70**, 026220. URL `http://link.aps.org/doi/10.1103/PhysRevE.70.026220`.

8. **Broussell, I.**, **I. L'Heureux**, and **E. Fortin** (1997). Experimental evidence for dichotomous noise-induced states in a bistable interference filter. *Physics Letters A*, **225**(13), 85 – 91. ISSN 0375-9601. URL `http://www.sciencedirect.com/science/article/pii/S0375960196008602`.

9. **Burnley, V.** and **F. E. C. Culick** (2000). Influence of random excitations on the acoustic instablities in combustion chambers. *AIAA Journal*, **38**(8), 8.

10. **Crocco, L.** and **S. Cheng**, *Theory of combustion Instability in Liquid Rocket Propellant Rocket Motors*. Butterworth's Scientific Publication, 1956.

11. **Crow, S. C.** and **F. H. Champagne** (1971). Orderly structure in jet turbulence. *Journal of Fluid Mechanics*, **48**(03), 547–591. URL `http://dx.doi.org/10.1017/S0022112071001745`.

12. **Darbyshire, A. G.** and **T. Mullin** (1995). Transition to turbulence in constant-mass-flux pipe flow. *Journal of Fluid Mechanics*, **289**, 83–114. URL `http://dx.doi.org/10.1017/S0022112095001248`.

13. **Deckker, B. E. L.** (1970). Evaluation of Rayleigh's Hypothesis in Low-Frequency Vibrating Diffusion Flames. *Acoustical Society of America Journal*, **47**, 1453.

14. **Dranovsky, M. L.**, *Combustion Instabilities in Liquid Rocket Engines: Testing and Development Practices in Russia. edited by V. Yang, F. E. C. Culick and D. G. Talley*. Progresses in Astronautics and Aeronautics, 2007.

15. **Duget, Y.**, **A. P. Willis**, and **R. R. Kerswell** (2008). Transition in pipe flow: the saddle structure on the boundary of turbulence. *Journal of Fluid Mechanics*, **613**, 255–274.

16. **Farrell, B. F.** and **P. J. Ioannou** (1994). Variance maintained by stochastic forcing of non-normal dynamical systems associated with linearly stable shear flows. *Phys. Rev. Lett.*, **72**, 1188–1191. URL `http://link.aps.org/doi/10.1103/PhysRevLett.72.1188`.

17. **Fedotov, S.**, **I. Bashkirtseva**, and **L. Ryashko** (2002). Stochastic analysis of a non-normal dynamical system mimicking a laminar-to-turbulent subcritical transition. *Physical Review E*, **66**, 066310.

18. **Harrje, D.** and **F. Reardon**, *Liquid propellant rocket combustion instability*. Number v. 7-12 in NASA SP. Scientific and Technical Information Office, National Aeronautics and Space Administration; [for sale by the Supt. of Docs., U.S. Govt. Print. Off.], 1972.

19. **Higgins, B.** (1802). On the sound produced by a current of hydrogen gas passing through a tube. *A Journal of natural philosophy, chemistry, and the arts*, **1**.

20. **Hohenberg, P. C.** and **J. B. Swift** (1992). Effects of additive noise at the onset of rayleigh-bénard convection. *Phys. Rev. A*, **46**, 4773–4785. URL `http://link.aps.org/doi/10.1103/PhysRevA.46.4773`.

21. **Horsethemke, W.** and **R. Lefever**, *Noise Induced transitions*. Springer-Verlag, New York, 1984.

22. **Hutt, A.** (2008). Additive noise may change the stability of nonlinear systems. *EPL (Europhysics Letters)*, **84**(3), 34003. URL `http://stacks.iop.org/0295-5075/84/i=3/a=34003`.

23. **Hwang, S. K.**, **J. B. Gao**, and **J. M. Liu** (2000). Noise-induced chaos in an optically injected semiconductor laser model. *Phys. Rev. E*, **61**, 5162–5170. URL `http://link.aps.org/doi/10.1103/PhysRevE.61.5162`.

24. **Ibrahim, R. A.** (2006). Excitation-induced stability and phase transition: A review. *Journal of Vibration and Control*, **12**(10), 1093–1170. ISSN 1077-5463.

25. **Jones, A. T.** (1945). Singing flames. *The Journal of the Acoustical Society of America*, **16**(4), 254–266. URL `http://link.aip.org/link/?JAS/16/254/1`.

26. **Juel, A.**, **A. Darbyshire**, and **T. Mullin** (1997). The effect of noise on pitchfork and Hopf bifurcations. *Proceedings of the Royal Society of London series A- Mathematical Physical and Engineering sciences*, **453**(1967), 2627–2647.

27. **Juniper, M. P.** (2011). Triggering in the horizontal Rijke tube: Non-normality, transient growth and bypass transition. *Journal of Fluid Mechanics*, **667**, 272–308.

28. **Kabashima, S.**, **S. Kogure**, and **T. Okada** (1979). Oscillatorytononoscillatory transition due to external noise in a parametric oscillator. *Journal of Applied Physiscs*, **50**(10), 6926–6302.

29. **Kim, K. T.** and **S. Hochgreb** (2011). Measurements of triggering and transient growth in a model lean-premixed gas turbine combustor. *Combustion and Flame*, **159**(3), 1215–1227. ISSN 0010-2180.

30. **Kinsler, L. E.**, **A. R. Frey**, **A. B. Coppens**, and **J. V. Sanders**, *Fundamentals of Acoustics*. John Wiley and Sons, Inc., USA, 2000, 4th edition.

31. **Klein, S. A.** (2000). *On the acoustics of turbulent non-premixed flames*. Ph.D. thesis, Enschede. URL `http://doc.utwente.nl/32033/`.

32. **Komarov, S.** and **M. Hirasawa** (2003). Enhancement of gas phase heat transfer by acoustic field application. *Ultrasonics*, **41**(4), 289 – 293. ISSN 0041-624X. URL `http://www.sciencedirect.com/science/article/pii/S0041624X02004547`.

33. **Lieuwen, T. C.** (2001). Phase drift characterization of self excited combustion driven oscillations. *Journal of Sound & Vibration*, **242**(5), 893–905.

34. **Lieuwen, T. C.** and **A. Banaszuk** (2005). Background noise effects on the combustor stability. *Journal of Propulsion and Power*, **21**(1), 25–31.

35. **Lieuwen, T. C.** and **B. T. Zinn** (2002). Experimental investigation of limit-cycle oscillations in an unstable gas turbine combustor. *Journal of Propulsion and Power*, **18**(1), 61–67. URL `http://doi.aiaa.org/10.2514/2.5898`.

36. **Lindner, B.**, **J. GarcÄśÌĄa-Ojalvo**, **A. Neiman**, and **L. Schimansky-Geier** (2004). Effects of noise in excitable systems. *Physics Reports*, **392**(6), 321 – 424. ISSN 0370-1573. URL `http://www.sciencedirect.com/science/article/pii/S0370157303004228`.

37. **Mariappan, S.**, **P. J. Schmid**, and **R. I. Sujith** (2010). Role of transient growth in subcritical transition to thermoacoustic instability in a horizontal Rijke tube. *16th AIAA/CEAS Aeroacoustics Conference, 7 - 9 June 2010, Stockholm, Sweden, AIAA 2010-3857*.

38. **Mariappan, S.** and **R. I. Sujith** (2010). Thermoacoustic instability in solid rocket motor - non-normality and nonlinear instabilities. *Journal of Fluid Mechanics*, **653**, 1–33.

39. **Mariappan, S.**, **R. I. Sujith**, and **P. J. Schmid**, Non-normality of thermoacoustic interactions: an experimental investigation. *In* 47^{th} *AIAA/ASME/SAE/ASEE Joint Propulsion conference, AIAA 2011-5555*. Sandiego,California,USA, 2011.

40. **Markstein, G. H.** and **W. Squire** (1955). On the stability of a plane flame front in oscillating flow. *The Journal of the Acoustical Society of America*, **27**(3), 416–424. URL `http://link.aip.org/link/?JAS/27/416/1`.

41. **Meunier, C.** and **A. D. Verga** (1988). Noise and bifurcations. *Journal of Statistical Physics*, **50**, 345–375. ISSN 0022-4715. URL http://dx.doi.org/10.1007/BF01022998. 10.1007/BF01022998.

42. **Mullin, T.** (2011). Experimental studies of transition to turbulence in a pipe. *Annual Review of Fluid Mechanics*, **43**(1), 1–24. URL http://www.annualreviews.org/doi/abs/10.1146/annurev-fluid-122109-160652.

43. **NAG, P. K.**, *Engineering Thermodynamics*. Tata McGraw-Hill Publishing Company Ltd, 2005.

44. **Nicoud, F.**, **L. Benoit**, **C. Sensiau**, and **T. Poinsot** (2007). Acoustic modes in combustors with complex impedances and multidimensional active flames. *AIAA. Journal*, **45**, 426–441.

45. **Noiray, N.**, **D. Durox**, **T. Schuller**, and **S. Candel** (2008). A unified framework for nonlinear combustion instability analysis based on the flame describing function. *Journal of Fluid Mechanics*, **615**, 139–167.

46. **Nori, V. N.** and **J. M. Seitzman.**, Chemiluminescence measurements and modeling in syngas, methane and jet-a fueled combustors. *In Forty-Fifth Aerospace Sciences Meeting and Exhibit*. AIAA, Reno, NV, 2007.

47. **Norton, M.** and **D. Karczub**, *Fundamentals of noise and vibration analysis for engineers*. Cambridge University Press, 2003. ISBN 9780521495615.

48. **Oh, J.** and **G. Ahlers** (2003). Thermal-noise effect on the transition to rayleigh-bénard convection. *Phys. Rev. Lett.*, **91**, 094501. URL http://link.aps.org/doi/10.1103/PhysRevLett.91.094501.

49. **O'Neill, P.**, **J. Soria**, and **D. Honnery** (2004). The stability of low reynolds number round jets. *Experiments in Fluids*, **36**, 473–483. ISSN 0723-4864. URL http://dx.doi.org/10.1007/s00348-003-0751-5. 10.1007/s00348-003-0751-5.

50. **Perko, L.**, *Differential Equations and Dynamical Systems*. Springer, 2009.

51. **Perry, E. H.** (1970). *Investigation of the T-Burner and its role in combustion instability studies*. Ph.D. thesis, California Institute of Technology, Pasadena, California.

52. **Putnam, A.**, **F. Belles**, and **J. Kentfield** (1986). Pulse combustion. *Progress in Energy and Combustion Science*, **12**(1), 43 – 79. ISSN 0360-1285. URL http://www.sciencedirect.com/science/article/pii/0360128586900134.

53. **Putnam, A.**, **C. Rodman**, **R. Hyatt**, and **A. S. of Mechanical Engineers**, *Elimination of combustion-driven oscillations in a large air heater*. American Society of Mechanical Engineers. ASME, 1967. URL http://books.google.co.in/books?id=jOHoSAAACAAJ.

54. **Putnam, A. A.**, *Combustion Driven Oscillations in Industry*. Elsevier, 1971, fuel and energy science series edition.

55. **Putnam, A. A.** and **W. R. Dennis** (1955). A survey of organ-pipe oscillations in combustion systems. *The Journal of the Acoustical Society of America*, **27**(5), 1014–1014. URL http://link.aip.org/link/?JAS/27/1014/4.

56. **Raffel, M.**, **C. Willert**, and **J. Kompenhans**, *Particle image velocimetry: a practical guide*. Experimental fluid mechanics. Springer, 1998. ISBN 9783540636830. URL http://books.google.co.in/books?id=dopRAAAAMAAJ.

57. **Rankin, G. W.**, **K. Sridhar**, **M. Arulraja**, and **K. R. Kumar** (1983). An experimental investigation of laminar axisymmetric submerged jets. *Journal of Fluid Mechanics*, **133**, 217–231. URL http://dx.doi.org/10.1017/S0022112083001871.

58. **Rayleigh, L.** (1878). The explanation or certain acoustic phenomena. *Nature*, **18**(319), 319–321. URL http://scholar.google.com/scholar?hl=en&btnG=Search&q=intitle:The+explanation+of+certain+acoustic+phenomena#0.

59. **Resch, P.**, **A. F. Muenster**, and **F. W. Schneider** (1991). A subcritical hopf bifurcation in the methylene blue oscillator: effects of imposed fluctuations. *The Journal of Physical Chemistry*, **95**(16), 6270–6275. URL http://pubs.acs.org/doi/abs/10.1021/j100169a039.

60. **Residori, S.**, **R. Berthet**, **B. Roman**, and **S. Fauve** (2002). Noise induced bistability of parametric surface waves. *Phys. Rev. Lett.*, **88**, 024502–1.

61. **Reynst, F.**, *Pulsating combustion: the collected works of F.H. Reynst*. Pergamom Press, 1961.

62. **Rijke, P. L.** (1859*a*). Notice of a new method of causing a vibration of the air contained in a tube open at both ends. *Philosophical Magazine Series 4*, **17**(116), 419–422. URL http://www.tandfonline.com/doi/abs/10.1080/14786445908642701.

63. **Rijke, P. L.** (1859*b*). On the vibration of the air in a tube open at both ends. *The London, Edinburgh and Dublin philosophical magazine and journal of science*, **17**, 419–422.

64. **Scientifique, L. L. D.**, *Gas Encyclopaedia*. Elsevier, 1976. ISBN 9780444414922.

65. **Sheen, H. J.**, **W. J. Chen**, and **J. S. Wu** (1997). Flow patterns for an annular flow over an axisymmetric sudden expansion. *Journal of Fluid Mechanics*, **350**, 177–188.

66. **Sondhauss, K.** (1850). Über die schallschwingungen der luft in erhitzten glasrohren und in gedeckten pfeifen von ungleicher weite. *Annalen der Physik und Chemie*, **79**, 1–34.

67. **Strogatz, S. H.**, *Nonlinear Dynamics and Chaos: with applications to Physics, Biology, Chemistry, and Engineering*. Westview Press, Colorado, 2000, 1st edition.

68. **Subramanian, P.** and **R. I. Sujith** (2011). Non-normality and internal flame dynamics in premixed flameâĂŞacoustic interaction. *Journal of Fluid Mechanics*, **679**, 315–342. URL http://dx.doi.org/10.1017/S0022112011001406.

69. **Sujith, R. I.** (2005). An experimental investigation of interaction of sprays with acoustic fields. *Experiments in Fluids*, **38**, 576–587. ISSN 0723-4864. URL http://dx.doi.org/10.1007/s00348-004-0912-1. 10.1007/s00348-004-0912-1.

70. **Swift, J.** and **P. C. Hohenberg** (1977). Hydrodynamic fluctuations at the convective instability. *Phys. Rev. A*, **15**, 319–328. URL http://link.aps.org/doi/10.1103/PhysRevA.15.319.

71. **Taconis, K.**, **J. Beenakker**, **A. Nier**, and **L. Aldrich** (1949). Measurements concerning the vapour-liquid equilibrum of solutions of he3 in he4 below 2.19řk. *Physica*, **15**, 733 – 739. ISSN 0031-8914. URL http://www.sciencedirect.com/science/article/pii/0031891449900786.

72. **Waugh, I. C.**, **M. Geuß**, and **M. Juniper** (2011). Triggering, bypass transition and the effect of noise on a linearly stable thermoacoustic system. *Proceedings of the Combustion Institute*, **33**(2), 2945 – 2952.

73. **Waugh, I. C.** and **M. Juniper** (2011). Triggering in a thermoacoustic system with stochastic noise. *International Journal of Spray and Combustion Dynamics*, **3**, 224–242.

74. **White, F.**, *Fluid Mechanics*. McGraw-Hill series in mechanical engineering. McGraw Hill, 2010. ISBN 9780077422417. URL http://books.google.co.in/books?id=d48lQwAACAAJ.

75. **Zaikin, A.** and **J. Kurths** (2000). Additive noise and noise-induced nonequilibrium phase transitions. *AIP Conference Proceedings*, **511**(1), 303–313. URL http://link.aip.org/link/?APC/511/303/1.

76. **Zhao, D.** (2012). Transient growth of flow disturbances in triggering a rijke tube combustion instability. *Combustion and Flame*, **159**(6), 2126 – 2137. ISSN 0010-2180. URL http://www.sciencedirect.com/science/article/pii/S0010218012000417.

77. **Zinn, B. T.** and **T. C. Lieuwen**, *Combustion instabilities: basic concepts. Combustion instabilities in Gas turbine Engines: Operational experience, Fundamental Mechanisms, Modeling*, volume 210. Progress in Astronautics and Aeronautics, New York, 2005.

78. **Zinn, B. T.** and **T. C. Lieuwen**, *Combustion instabilities: Basic concepts - Combustion Instabilities in Gas Turbine Engines: Operational Experience, Fundamental Mechanisms, and Modeling*. AIAA, USA, 2006.

LIST OF PAPERS BASED ON THESIS

1. Jegadeesan, V. and Sujith, R. I. Experimental Investigation of Noise Induced Triggering in Thermoacoustic System, Accepted for oral presentation and proceedings of *34th International Symposium on Combustion.*, 2012, Warsaw, Poland